Power and Thermal Characterization of a Lunar Weather Station and Laser Space Communications Network Node

a project presented to
The Faculty of the Department of Aerospace Engineering
San José State University

in partial fulfillment of the requirements for the degree
Master of Science in Aerospace Engineering

by

Avraham S. Gileadi

May 2023

approved by

Ali Guarneros-Luna
Faculty Advisor

ABSTRACT

Power and Thermal Characterization of a Lunar Weather Station and Laser Space Communications Network Node

by Avraham S. Gileadi

With the advent of new launch capabilities and new crewed missions, it is expected that surface-based mission concepts will change significantly, especially for the Moon. Deep space communications infrastructure is about to see an expansion in capabilities and technology. A new emphasis on optical communications is driven by the increased bandwidth needs of scientific missions. Communication systems that can receive, store, and retransmit data are needed to support a system that is inherently intermittent. The equipment proposed by this paper stands where the new realities meet. A lunar communications station would require continuous power for operations and would be installed near significant lunar infrastructure. Scientific equipment such as seismometers could also be included, enabling advanced warning of potential ejecta hazards from nearby meteoroid impacts. Dual optical modules would provide communications relay capabilities in a predictable location with good visibility. Any long-duration lunar system needing to sustain operation through the long and cold lunar nights requires an innovative approach. This project compares the use of regolith as thermal insulation with a more conventional approach to insulation.

Acknowledgements

I would like to acknowledge and thank my mentor Ali Guarneros-Luna for the support in bringing this ambitious project into existence. Having someone who was willing to go on this journey with me provided a huge confidence boost. Thank you to San Jose State University for giving me the opportunity to explore my passion. Thank you to my mentors in the FML at NASA Ames Research Center for believing in me and helping with good ideas and positivity.

I thank my daughter Ava for understanding that worthwhile things take diligence and hard work. My family has provided so much encouragement and constant support, thank you for all the help.

Table of Contents

List of Figures

Symbols

Symbol	Definition	Units
q_k	Conductive heat transfer rate	W/m^2
q_r	Radiative heat flow	W/m^2
q_c	Convective heat transfer	W/m^2
$\bar{h}_c$	Average heat transfer coefficient	W/ (m^2 K)
A	Heat transfer area	m^2
k	Thermal conductivity	W/ (m K)
T	Temperature	Kelvin
t	Time	Seconds
x	Distance	m
L	Length	m
σ	Stefan-Boltzmann constant	W/ (m^2 K^4)
ε	Emittance	unitless
F	Shape factor	unitless
ν	Diffusivity coefficient	unitless
α	Air speed	m/s

1. Introduction

1.1 Motivation

For the first time in fifty years, the world is once again pursuing crewed space missions outside of low Earth orbit. With the advent of new launch systems including SLS, Starship and others, as well as a renewed public interest in space, the options for research opportunities and capital investment available to students and entrepreneurs appears on track to reach an all-time high. These new systems bring with them new capabilities, expanding the envelope of what kinds of missions are possible. At the same time, the development of enabling technologies that will be used for space missions have also been advancing at a rapid pace.

Free-space optical communications (or laser communications) have already demonstrated deep-space downlink speeds as high as 622 Mbps with an uplink speed as fast as 20 Mbps, and come with a significant reduction in size, weight, and power requirements [1]. There are already plans to augment NASA's Deep Space Network (DSN) with laser communications modules [2]. This technology also has scientific research potential as the architecture could be used to significantly improve the accuracy of laser ranging of the Moon [3]. Currently, ranging of the Moon is performed using high powered lasers from terrestrial observatories and retroreflectors on the lunar surface, an effort made significantly harder because of the refraction from Earth's atmosphere. When using a Moon-based system, laser light would only have to transit the atmosphere once, a substantial improvement. The likelihood of installation of a laser communications system on the lunar surface seems high considering the plans NASA has for the Moon.

NASA has plans to establish an outpost on the Moon that can be used as a proving ground for technologies to be used in deep-space exploration. These plans include extended duration missions on the lunar surface. One of the hazards that astronauts will face on the lunar surface will come from meteoroid strikes. Meteoroids strike the lunar surface with enough momentum to kick up ejecta that can land far from the impact side. As the Moon has little gravity or atmosphere, the hazards from ejecta can be as serious as those posed by the meteoroids themselves. Currently, the primary method of determining the location of impacts uses terrestrial based telescopes that look for bright flashes on the lunar surface, an indication of a meteoroid impact [4]. An improvement on this method would be to station multiple satellites in lunar orbit to look for impact flashes. Observations could be used to provide early warning of hazards from ejecta to astronauts and facilities. A further improvement would be to station multiple seismometers on the lunar surface to triangulate the exact size and location of impacts. The technologies and methods for surfaced based seismometers have been studied extensively in the context of a lunar geophysical network [5]. Significant meteoroid strikes are happening all the time on the Moon [4]. Together with data from lunar orbiters, a seismometer network can provide high accuracy ejecta "weather" forecasts to countries conducting lunar operations.

Despite the advances in technology, the cost to deliver payloads to the lunar surface is likely to remain a primary mission selection consideration. The system studied in this thesis project addresses cost in the following ways. It combines two systems that are likely to be in high demand on the Moon in the future: an optical communications network node and a geophysical network node. The result is a reduction in cost, size, and complexity as significant components can be shared between the systems. Furthermore, the system is intended to be delivered as cargo

as a part of a crewed mission, eliminating the need for a dedicated launcher and lander. This last consideration also reduces risks associated with proper installation of the seismometers.

The primary problems considered by this thesis are the cold temperatures, and the availability of sunlight and their effect on permanently installed hardware. Hardware installed in the mid and low latitudes will have to survive for 336 hours (14 days) without sunlight whereas hardware installed at the south pole will only have to endure for 60-100 hours without sunlight [6]. It follows that all landing sites for planned crewed missions to the lunar surface will be at the south pole [10], so thermal and power considerations will be evaluated for this environment. Because a robust communications and seismometer network will require multiple installations, the environment of the low / mid-latitudes will also be considered. It is also a hope that the knowledge gained from this project can translate to the development of continuously inhabited lunar human habitation systems. Understanding the power and thermal requirements for hardware to survive for long durations on the lunar surface will be an important consideration for the hardware proposed by this thesis, and for any long-duration extra-terrestrial surface installation.

1.2   Literature review

1.2.1   Lunar Temperatures

The thermal environment on the Moon is primarily driven by the amount of incident sunlight the surface absorbs, which is a function of the location, topology, albedo of the surface and the composition of the regolith [7]. Temperatures recorded by the Diviner Lunar Radiometer Experiment (shown below in Figure 1.1, Figure 1.2, and Figure 1.3) show the sizable impact that latitude has on the surface temperature.
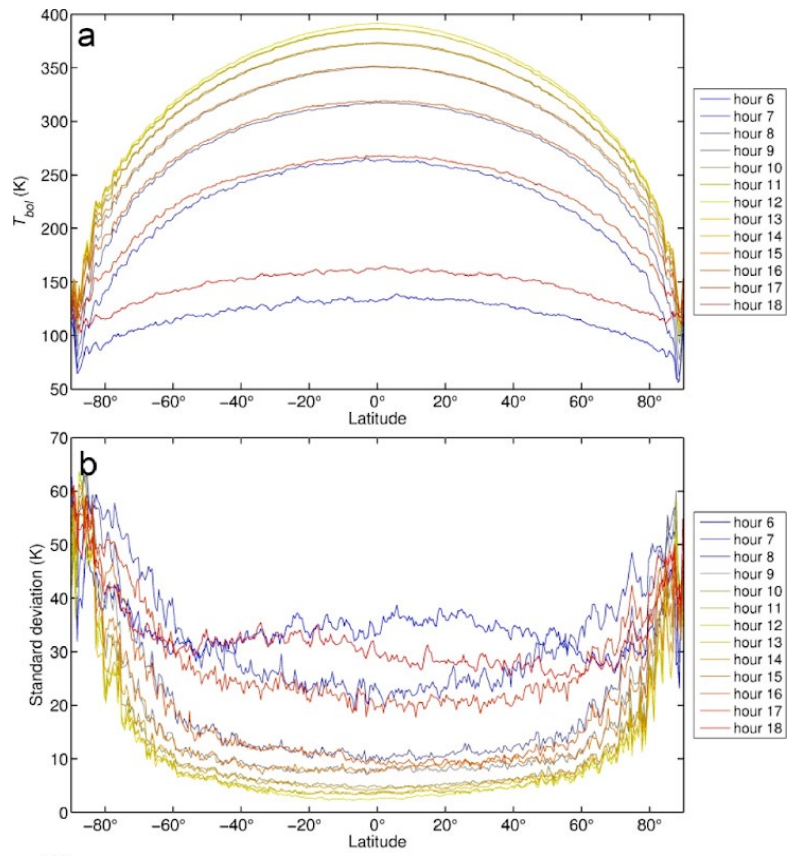
Figure 1.1 - Mean hourly daytime temperatures [7]
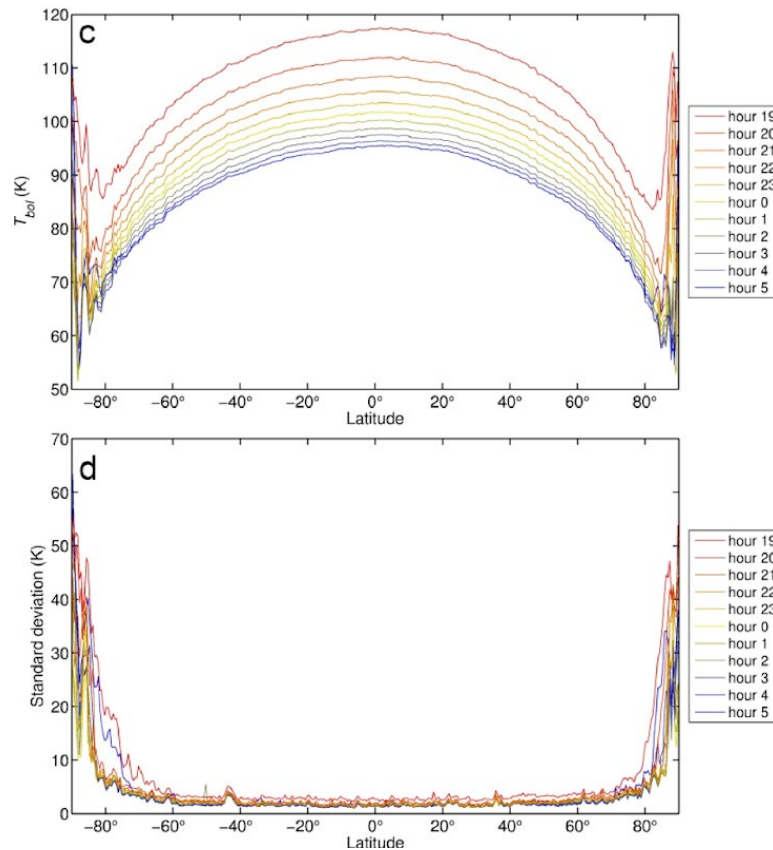
Figure 1.2 - Mean hourly nighttime temperatures [7]

These measurements come with large standard deviations. The standard deviation for daytime temperatures measurements ranged between 5-40 K at the equator and 30-60 K at the poles. The standard deviation for nighttime temperatures measurements are approx. 5 K at the equator and 20-50 K at the poles.

1.2.1.1 Lunar South Pole

There are craters at the south pole that, due to the combination of the oblique angle of sunlight and crater depth, never see sunlight. Characterizing the thermal environment is challenging. Average temperatures range between 50 K (dark crater locations) and 202 K, but due to the large number of influencing factors, averages may not be indicative of actual conditions. There are plateaus and ridges with elevations as high as 7010 meters and valleys as deep as -5480 meters [8]. The size, orientation, and height of the slopes relative to the Sun is a significant variable. There is a strong correlation between the maximum temperatures and the amount of sunlight the location receives. The absolute maximum temperatures can reach as high as 350K at higher elevations that receive more sunlight [8]. Equipment installed at the south pole will likely have location specific designs.
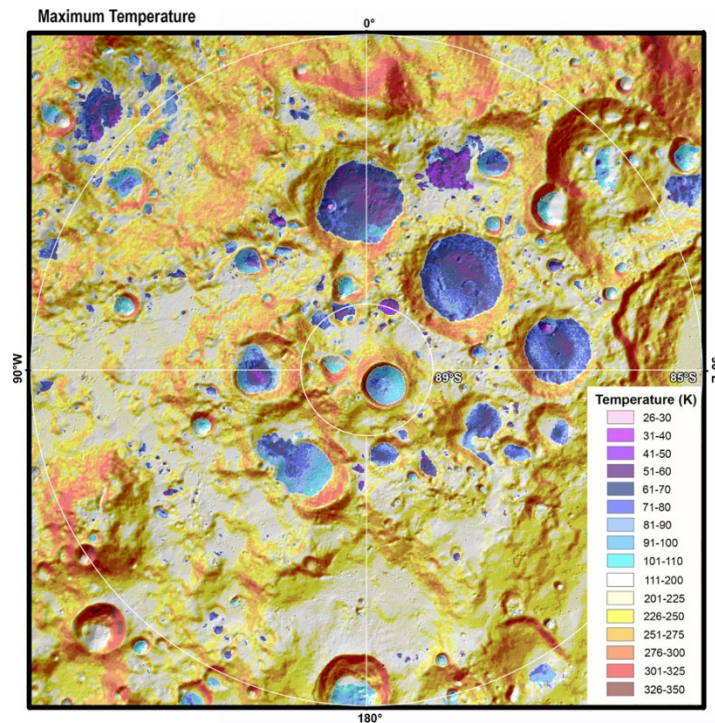
Figure 1.3 - Maximum temperatures at latitudes greater than 85° (south pole) [8]

1.2.1.2 Low and mid latitudes

During daylight hours, low and mid latitudes are characterized by vast regions with continuous sunlight. As a result, maximum temperatures are highest in the lower latitudes, reaching as high as 392.3 K at the equator with lows dropping to as low as 94.3 K at night [7].

1.2.1.3 Sub-surface

Lunar regolith has a low bulk density at 1.75-2.09 g/cm^3 and is not very thermally conductive at 1.6 W/cm^2 [9]. Regolith is a good insulator against the large temperature swings seen on the surface. Temperature probes installed by astronauts on the Apollo 15 and Apollo 17 missions measured sub-surface temperatures at various depths over multiple years. Figure 1.4 below shows that subsurface temperatures at a depth of 1 meter ranged between 249 and 255.5 K over the course of the multi-year experiment [9].

Analysis found that the temperature of regolith at some locations was influenced by higher concentrations of Thorium [9]. Topography and regolith composition are also factors, but for the purposes of the system discussed in this project thesis, impacts from regolith compositions and topography will be neglected.
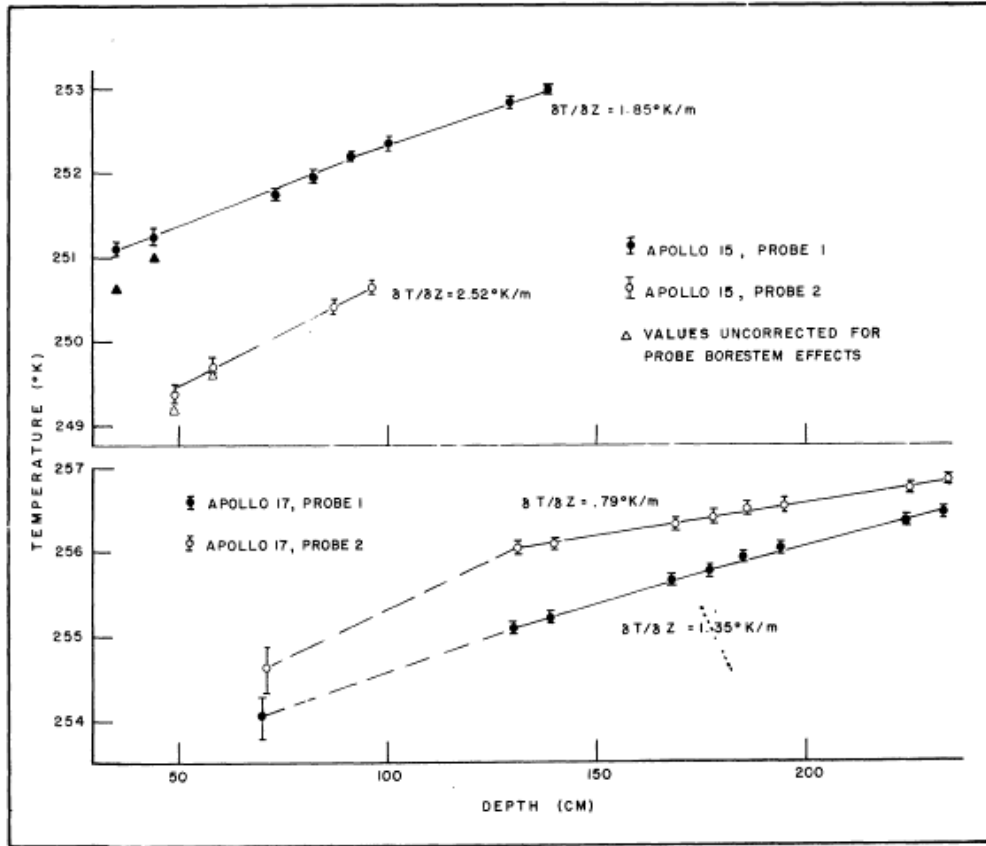
Figure 1.4 - Apollo measurements of sub-surface temperatures [9]

1.2.2 Solar Power Availability

1.2.2.1 South Pole

Because the Moon's rotation angle is just 1.54°, some locations at higher elevations at the south pole experience long periods of continuous sunlight broken up by relatively short periods of dark [6]. There are a very limited number of sites where sunlight is plentiful, and periods of dark are minimized. The number increases quickly as tolerance for longer durations without sunlight increases.

A study conducted by Vanoutryve et al. [6] for the European Space Agency (ESA) identified one south pole site with over 300 days of continuous illumination, eight sites with over 200 days of continuous illumination, and three with over 170 days of continuous illumination. In their study, researchers analyzed laser altimeter data collected by the Kaguya spacecraft as well as positional data for the Earth and Moon relative to the Sun in 2018. Feeding the data into MATLAB, they analyzed the line-of-sight conditions for high altitude locations relative to the Sun and Earth. Their study found that some of the best sites were dark for just 60 hours, with many more options available as tolerance for no-light periods increased to 100 hours [6]. It is likely that the locations with long continuous light periods and short no-light periods will be highly coveted as systems in these locations can be cheaper and lighter. It appears that there will

be areas adjacent to the premium locales where smaller systems with high no-light survivability could be installed.

NASA has performed studies of the south pole and published candidate regions for exploration [10]. Plotting the NASA and ESA locations on a topographic map [8] shows close alignment between the two space agencies. See Figure 1.5 below. This is a strong indication that there will be competition between all space agencies in securing the locations with the best light.
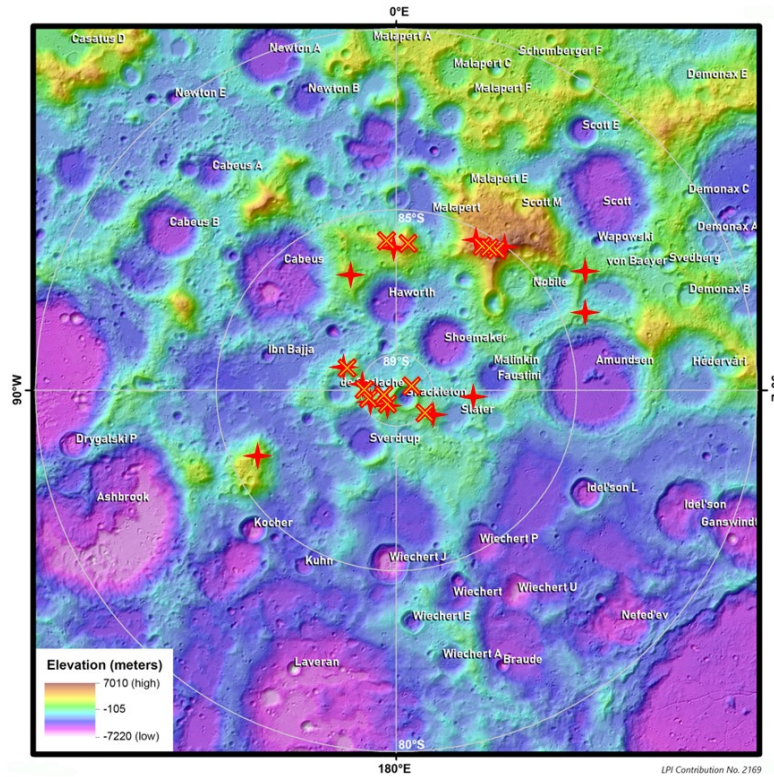
Figure 1.5 - South pole topographical map with NASA (✦) and ESA (×) candidate regions plotted [8][6][10]

1.2.2.2   Low and Mid Latitudes

Analyzing the availability of sunlight in the low and mid latitudes is straightforward. Lunar day lasts approximately 14 days and that is followed by 14 days of lunar night. The constraints that come with designing a system that can survive extreme cold temperatures and long dark durations are significant.

1.2.3   Laser Communications

1.2.3.1   Overview

Optical communications offer many advantages over traditional Radio Frequency (RF) communication systems. Optical systems operate in the infrared with a much shorter wavelength than RF systems. This provides significantly higher data rates. Optical systems typically employ lasers which are highly directional. When combined with telescopes, the signal can

transit very long distances while preserving high photon density. This makes the signal very power efficient and resistant to being intercepted. As the carrier signal is light, the modulation bandwidths are much larger which further improves efficiency [11].

Having multiple ground stations on Earth that are properly set up for optical communications is an important consideration. The refractive nature of Earth's atmosphere has a serious impact on the apparent strength of the laser signal. Clouds and weather are also a factor as they can block signal reception. Ground stations should be equipped with relatively large optics, high efficiency detectors, and Adaptive Optics (AO). AO systems use high frequency mechanical deformation of mirrors to compensate in real time for the distortions in the signal caused by the ever-changing refractive index of Earth's atmosphere and greatly improve the signal to noise ratio.

1.2.3.2 Line of Sight Availability at the South Pole

Laser communications are fundamentally line of sight and, while the south pole may be an ideal location from a power availability standpoint, it is a challenging location from a communications standpoint. The Earth will set every 14 days and be hidden from view. Vanoutryve et al. [6] describe the problem as follows "Viewed from the poles in particular, the Earth describes an extended eight-shape, ranging between ±6.5º in elevation with regard to the local horizon, and ±8º in azimuth. Without considering terrain, the Earth would be in visibility during 14 days, and hidden the next 14 days."

Communications systems located at the south pole wishing to communicate with Earth will have to use satellites and stations orbiting the Earth and Moon to relay the signal. Having communications systems that are compatible with both the Deep Space Network and next generation optical communications networks will be a requirement.

1.2.3.3 Lunar Lasercom Space Terminal and Lunar Atmosphere and Dust Environment Explorer

The Lunar Lasercom Space Terminal (LLST) aboard the Lunar Atmosphere and Dust Environment Explorer (LADEE) satellite successfully demonstrated that high bandwidth communications from lunar orbit was possible. To accomplish this goal, the satellite needed to hold a very tight attitude while the gimballed and inertially stabilized communications system acquired and tracked ground stations on Earth. The LLST system successfully demonstrated 39-620 Mbps downlink and 10-19 Mbps uplink speeds using a 100 mm telescope mounted to the exterior of LADEE [12].

The LLST system consists of a modem, controller electronics and optical module. Together, the optical module and controller electronics of LLST weigh 19.04 kg and consume ~12 W [11] [12]. The modem measures 315 x 261 x 185 mm, weighs 10.96 kg, consumes ~78 Watts, and was built largely from off the shelf components which were validated for launch and operation in space [12]. The pump laser drivers consist of continuous wave DFB lasers with Erbium-doped fiber amplifiers and are thermally stabilized using temperature stabilized Fiber Bragg Gratings [12]. It's worth pointing out these systems are used in common terrestrial fiber optics communications systems.

The temperature of the pump laser drivers has a significant impact on the transmitter output power and wavelength. A 40°C swing in temperature reduced the power at 1,200 mA by as much as 10% and shifted the center wavelength of the laser by as much as 10nm

[12]. Temperature control of the lasers used for downlink communications is an important consideration for laser communications systems.
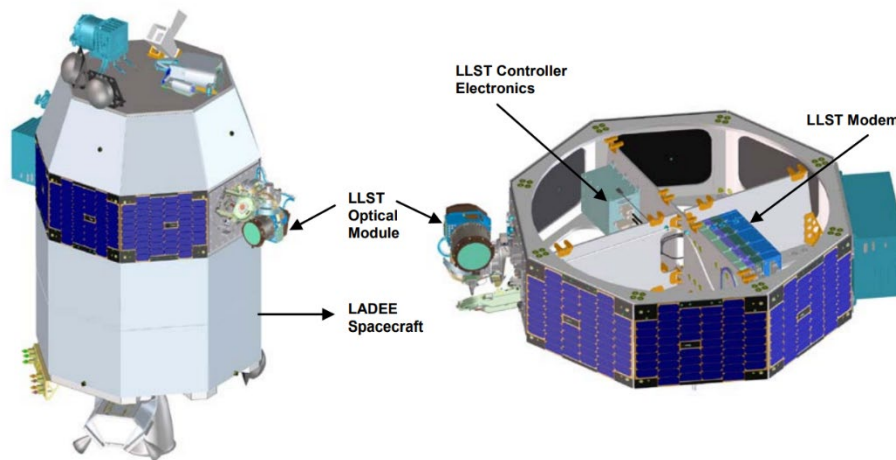
Figure 1.6 - LLST on the LADEE spacecraft

1.2.3.4 *Laser Communications Relay Demonstration*

The Laser Communications Relay Demonstration (LCRD) is NASA's next step in developing an optical communications network after LLST. The system was launched onboard the STPSat-6 spacecraft in 2021 [2]. Unlike LADEE, its mission will last multiple years and provide operators an opportunity to build on and develop the architecture. LCRD operates in geostationary orbit and is intended to demonstrate speeds between 311 Mbps and 1.244 Gbps. A review of the papers published for the system failed to obtain power and size specifications for the system. LCRD is equipped with two gimballed optical communication terminals and will have the capability to relay signals. LCRD includes a Secure Host Interface Unit (SHIM) to provide data encryption [2].

Figure 1.7 - LCRD on the STPSat-6 spacecraft [2]

1.2.3.5 CubeSat Laser Infrared CrosslinK

The CubeSat Laser Infrared CrosslinK (CLICK) mission will demonstrate laser communications between two CubeSats in low Earth orbit and was launched to the International Space Station in 2022. They hope to demonstrate a crosslink communications rate of 20 Mbps with satellite distances ranging between 25 and 580 km [13]. The CLICK module is installed aboard an Attitude Determination and Control System (ADCS) which provides coarse pointing functionality. Fine pointing functions are provided by MEMS fast steering mirrors [13]. The CLICK payload measures 96 x 147 x 96 mm, weighs 1.5 kg, and consumes ~ 30 W during full-duplex lasercom [14].
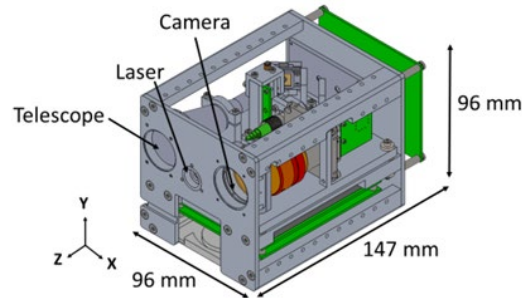
Figure 1.8 - CLICK payload [14]

1.2.3.6 European Space Agency Systems

ESA has been using lasers for communication for years. Their systems are heavier and more expensive than the systems discussed previously and use different wavelengths, making them incompatible with NASA's systems. TESAT's SCOT80 laser communications terminal for satellite networks provides 10 Gbps bidirectional communications at 8,000 km. It does this at a size of 500 x 180 x 260 mm for the optical head and 260 x 110 x 175 mm for the electronics package, mass of 15 kg, and with a power consumption rate of 60-80 W [15].

Figure 1.9 - TESAT SCOT80 Laser Communications Terminal [15]

1.2.4 Lunar Dust Management

Dust transportation mechanisms include regolith displacement from meteoroid impact, electrical potential from ionization and electrostatic charging of the surface, surface activities [36]. Optical surfaces can be treated in a lab prior to commissioning to reduce adhesion. Adhered lunar dust can be cleaned using a jet of fluid (CO_2 or inhibisol methyl chloroform) or mechanically with a brush accompanied by a gas jet [36]. Electrodynamic Dust Shield (EDS) and Electrostatic Lunar Dust Repeller (ELDR) use electrical fields to repel charged lunar dust particles. It has been shown that EDS combined with ultrasonic vibration is effective at removing dust from optical surfaces [36]. EDS and ELDR are likely to be primary methods for dust control, but the technology is largely unproven. Ideally the first installations of the equipment proposed by this paper would be in locations that could be monitored and maintained by astronauts until there is more use history for new technologies.

1.2.5 Thermal Switches

Thermal (heat) switches function by controlling heat conduction between two surfaces, typically the hardware requiring temperature control and thermal radiators [37]. Electronic equipment installed on the surface must be insulated from thermal radiators at night to conserve heat energy from the cold dark lunar environment. During the day, conduction between electronic equipment and the thermal radiators is required to dissipate the thermal loads. Passive thermal switches could provide this functionality. When cold, the two ends of the switch are separated by a gap, largely eliminating conduction. When exposed to heat the switch extends, closing the gap and providing conduction [37].
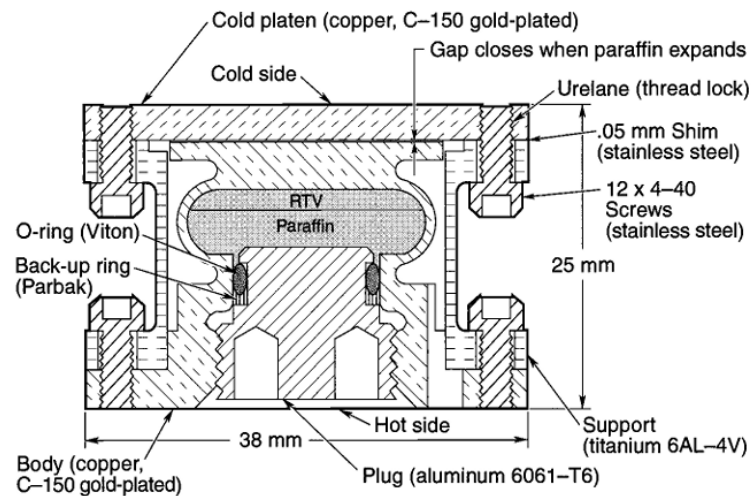
Figure 1.10 - Pedestal heat switch [37]

1.2.6 Lunar Geophysical Network

The mission of NASA's Lunar Geophysical Network (LGN) is to establish a network of science stations mounted to lunar landers. Each lander is outfitted with seismometers, heat flow

probes, retroreflectors, and magnetotelluric sounders that would be used to develop an understanding of the formation and evolution of our Moon and Earth as well as monitor meteoroid impacts to the lunar surface [5].

The mission concept is highly developed, and the mission definition includes extensive specifications for the equipment. Some relevant specifications are discussed here. Each lunar lander is equipped with four close range cameras and a panoramic imager. Together these weigh 9.8 kg and consume 25.8 W. X-band high-gain RF communications utilize a 0.5 m gimballing 28.9 dBi antenna requiring 17 W of power. The authors estimate 10 kg of batteries are required for each watt of power during the lunar night. They estimate heaters needed to keep the seismometer and cameras warm will consume 0.08 and 0.12 W respectively. The landers make use of 7.6 m² of solar cells (TJGaAs) which are expected to generate 800 W of power at the beginning of life and 700 W of power at end of life, 6 years later [5].

1.2.6.1 SI-Audio (SI) seismometer

This seismometer is approximately 50 mm in diameter, weighs 9.4 kg, and consumes an average of 4.6 W [5]. The creators believe this seismometer can capture low noise signals across a frequency range of 0.005 Hz to 400 Hz and is intended to be buried under 1 meter of lunar regolith [16].

Figure 1.11 - Silicon-Audio seismometer [17]

1.2.6.2 Very Broad Band (VBB) seismometer

This seismometer is 420 x 448 mm in size, weighs 25 kg and consumes an average of 11 W. Further requirements include temperature control between -55°C and +125°C. The very low frequency bandwidth signal measured by this sensor (1mHz / 25 Hz) can detect seismic waves the other seismometers cannot [5].
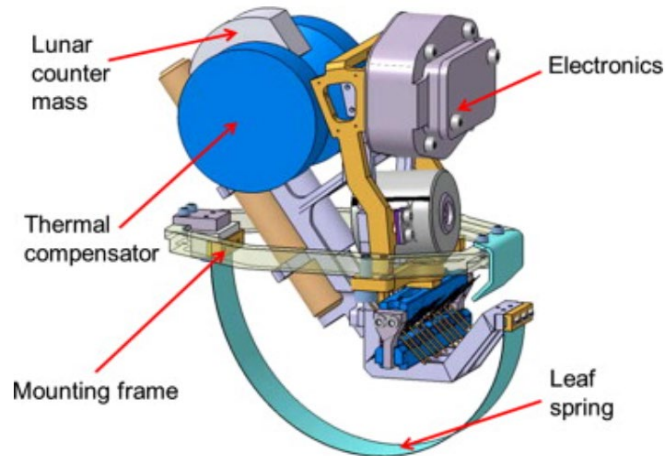
Figure 1.12 - Very Broad Band seismometer [16]

1.2.6.3 *Short Period (SP) seismometer*

This seismometer is 50 x 60 x 60 mm in size for a typical three-axis package, weighs 1 kg, and consumes an average of 2 W. Benefits of this seismometer are its durability, cost, and broad functionality [5].
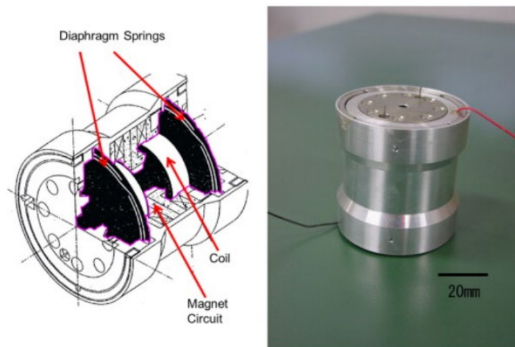
Figure 1.13 - Short Period seismometer [17]

1.2.7 Meteors and Meteoroids

Meteoroid impacts on the lunar surface have been studied using telescopes. Meteoroid impacts can be seen as bright flashes of light. The intensity and wavelength of the light can be measured and used to determine the size of the meteoroid [4]. Using data collected over the course of 20 years, researchers plotted the size distribution of meteoroids impacting the lunar surface.

In a study conducted from 1984 to 2006, Dubietis and Arlt [12] propose that variation in rate of meteor observations on Earth is a function of the minimum mass detectable by radar, which is correlated with solar activity. The Zenithal Hourly Rate (ZHR) of observations for the study, which are equivalent to observations made by a single observer under optimum conditions, are shown below. A mean hourly rate of 10 meteors per hour will be used.
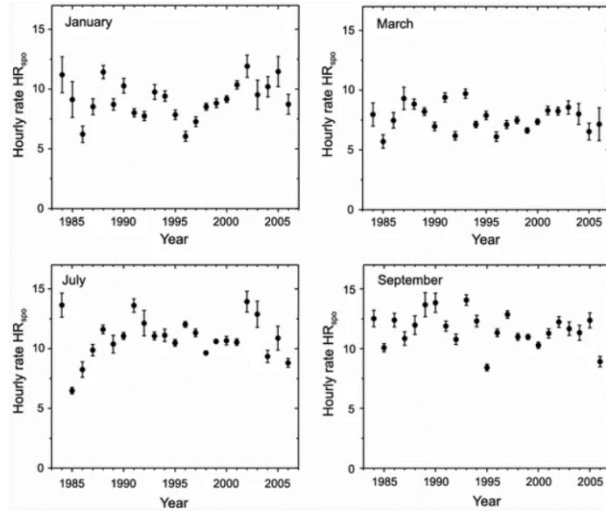
Figure 1.14 - Variability of visual sporadic meteor hourly rates in Earth's atmosphere [18]
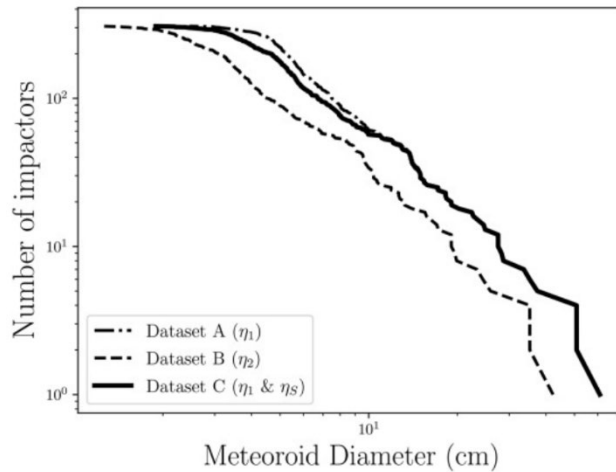
Figure 1.15 - Size distribution of lunar impacting meteoroids [4]

To estimate the hourly rate of meteoroid impacts on the lunar surface, we need to estimate the area of the Earth covered by the above observations and correlate that to the Moon. We will assume the area covered by the observations is equal to the area of a circle with the diameter of the Earth. The area covered by a circle with the diameter of the moon is 7.4% that of the Earth, so it is estimated that the sporadic meteoroid hourly rate on the Moon would be 7.4% that of the Earth, or roughly 0.74 impacts per hour. Over an 87,600-hour period (6 years), that equates to 64,824 impacts. Dividing this number of impacts over a cross sectional area of the Moon gives 0.0041 impacts per square kilometer over a 6-year period.

1.3 Project Proposal

This project will evaluate the benefits of using lunar regolith as insulation for equipment. The hope is it will provide a buffer against the extreme temperature swings on the surface as compared to typical architectures. The studied use case will be surface installation of

14

surface and subsurface hardware in both polar and mid-latitudinal locations. The study will focus on the thermal and power requirements of the hardware, evaluating the temperatures of the surface and subsurface hardware, as well as available power throughout a full lunar day/night cycle. The internal temperature of the hardware is intended to be held within a tolerance. Results for a system using regolith as insulation will be compared to one that does not. Power and thermal requirements will be scoped to service a remotely operated science and communications station. The science equipment functionality will be benchmarked against NASA's proposed lunar geophysical network hardware and the communications functionality will be benchmarked against NASA's LLST hardware with laser and RF components.

1.4 Methodology

Scoping and defining tasks will be accomplished by completing literature reviews, and by developing analysis and requirements documentation. Flight hardware is not a deliverable for this project thesis.

1.4.1 Power models

Models for power generation and consumption for equatorial and polar regions will be developed using MATLAB. This will include representative RF communication requirements as the communications hardware uses the most power for a given data rate. Power models will mimic those created for NASA's Lunar Geophysical Network (LGN) lander, seen in Figure 1.13 below.
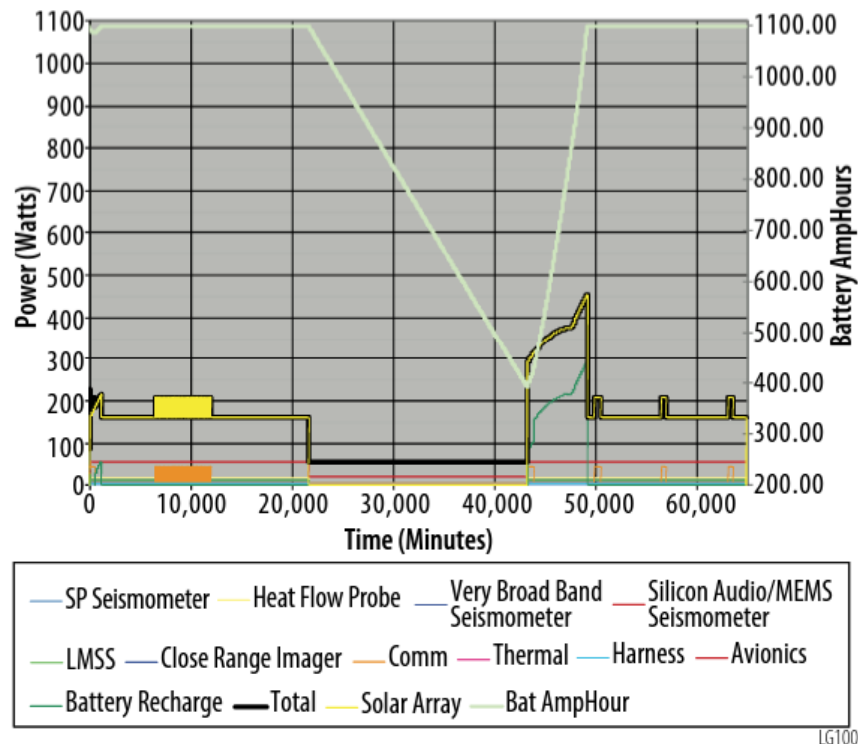
Figure 1.16 - Power consumption model for NASA's LGN lander [5]

1.4.2   Thermal simulation

    Computational Fluid Dynamics (CFD) analysis will be used to evaluate the thermal conditions. Representative hardware will be built and tested to validate the models. Thermal analyses will mimic those created for NASA's Lunar Geophysical Network (LGN) lander, seen in Figure 1.14 below.
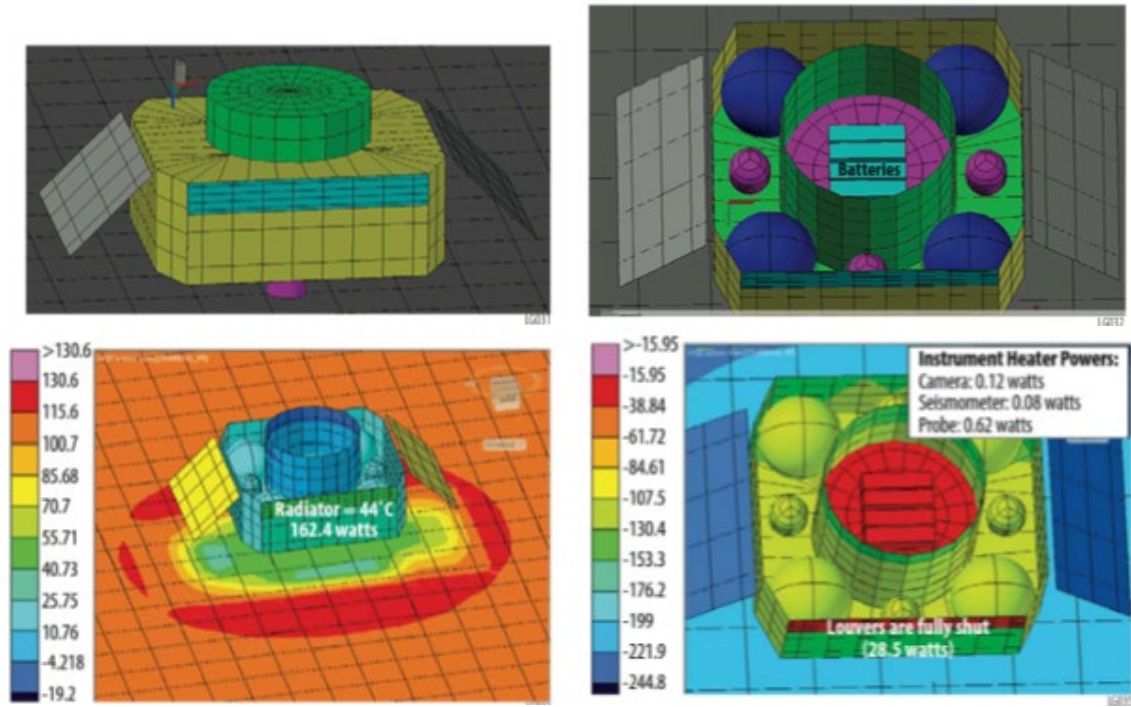
Figure 1.17 - Thermal analysis for NASA's LGN lander [5]

2. System Analysis and Design Considerations

2.1 Operational Concepts and Initial Sizing

2.1.1 Seismometers for Early Warning of Meteoroid Impacts

Meteoroids can cause damage in two ways: direct impact and secondary impacts from ejecta. The likelihood of a direct impact is exceedingly low. The low gravity and extremely sparse atmosphere of the moon means ejecta will travel long distances and fall at high velocities. The probability of a secondary impact from ejecta may be significant. As can be seen in the lunar meteoroid size distribution figure in the Literature Review section, a significant number of these meteoroids will be 10 cm or larger.

This equipment is intended to be installed as part of a larger operation that aims to establish a lunar base, and it is expected this equipment will be the only system equipped with seismometers. While the seismometers included with this system could be integrated into a geophysical network and could be used to triangulate impact locations and help map the interior of the Moon, initially the system will have to estimate the danger from flying ejecta based on the relative strength of the impact signal on the local seismometers. The seismometers would pick up P waves and S waves from the impact which are both within the operating range of SI-Audio and SP seismometers discussed in the Literature Review [30][31]. These sensors are both smaller, cheaper, and consume less energy than the VBB seismometer and will be sufficient to provide impact monitoring.

2.1.2 Communications, Optical and RF

The inclination of the Moon's equator relative to the ecliptic is 1.5°, and the inclination of the Moon's orbit relative to the Earth's orbit is 5.145° [19]. This has the effect of causing the Earth to wander in the sky when viewed from the surface of the Moon, the shape describing a figure 8. Optical and RF communication systems are both highly directional and will have to account for the movement.

The optical tracking system will require rough and fine motion control. On satellites, rough pointing is accomplished with two axis gimbals, or by pointing using the satellite attitude. Fine pointing is accomplished using the gimbals or using MEMS fast-steering mirrors. The lunar surface presents an added difficulty as the regolith will contaminate and jam unprotected mechanical actuators. It is anticipated a pointing system will be enclosed to keep out the dust, and the power requirements for both rough and fine pointing will be generally equivalent to a two-axis gimbal. The laser communications terminal is intended to operate as a relay, so two optical communications systems will be installed. The LLST system can achieve downlink rates between 39 and 620 Mbps, depending on the PPM slot rate [12]. When communicating with spacecraft, it is expected that the downlink speeds will reach 620 Mbps. When communicating with ground stations on Earth, the downlink speeds will vary depending on atmospheric conditions. An average downlink speed of 330 Mbps will be used. These numbers may be quite conservative as newer laser communications systems are in the process of demonstrating technologies that substantially increase speeds.

The Lunar Reconnaissance Orbiter (LRO) was designed to use s-band for tracking, telemetry, and commanding. This system weighs 8.8 kg. The LRO's S-band communications system provides 10 Mbps downlink and 4 Kbps uplink [20]. A representative high gain antenna will be

used in the design which weighs 0.1 kg and measures 8 x 8 x 1 cm [21]. A representative radio weighs 1 kg, measures 16 x 11 x 4.4 cm, and consumes 18 W at 28 VDC [22]. The high gain antenna and radio require thermal control.

2.1.3   Misc. Components

The size, mass, and power requirements for additional components are shown in the table below.

Table 2.1 - Size and power requirements for various components

Component	X [cm]	Y [cm]	Z [cm]	m [kg]	P_Active [W]	P_Inactive [W]	Reference
Controller	9	9.6	1.7	0.13	1.3	1.3	28
Camera	10	10	6.5	0.4	4.5	0	25
GPS Receiver	9	9.6	1.5	1	1	0	26

2.1.4   Photovoltaic Cells

Solar panels will be sized to supply ample power to support a heavy communications duty cycle during sunlight hours, as well as charging the batteries. Having a safety margin built-in will protect the system against unforeseen performance problems and ensure a long service life. The peak power consumption is estimated to be around 150 W, but many subsystems will not be active continuously. The photovoltaic panels will be required to fully charge the battery in as little as 328 hours (14 days). A suitable system would weigh 1.8 kg, measure 80 x 60 cm, and provide 132 W [24]. Depending on the size of the battery and safety margins, a larger panel may be required to completely charge the battery within 14 days.

2.1.5   Power Control Unit

Initial estimates indicate peak power consumption during the day (not including battery charging) will approach 150 W. This level of power draw during the night is not possible as the system will have to rely solely on battery power. With communications systems inactive, it is estimated the system will consume 15 W including heaters. Communication capability will be necessary at night but will happen on a reduced duty cycle. A representative power control unit that provides power distribution and battery management system weighs 3.3 kg, measures 14.7 x 24.9 x 12.3 cm, and consumes 10 W [23]. To reduce battery size, a second power control unit will be used. The night-time power distribution system weighs 2.45 kg, measures 16.7 x 26.7 x 8.9 cm, and consumes 4 W [29].

2.1.6   Battery

The battery chemistry chosen for the system is lithium-ion. Lithium-ion batteries were chosen because of their extensive use in space systems, high energy density, and because they operate at temperatures ranges like those that support life. Lithium-ion batteries degrade when charged to 100% or discharged near 0%. The pack will be designed to operate between 20% and close to 100% state of charge. Lithium batteries are known to degrade with each cycle. Over a 6-year mission, the battery will have to go through 146 charge-discharge cycles. It is expected the battery will lose less than 10% of its capacity from charge-discharge cycles if proper pack

temperatures are maintained. The primary job of the battery is to provide DC power when solar power isn't available. The battery will have to supply power for 328 hours at the equator and as long as 100 hours at the poles. A battery that needs to provide an average of 12 W for 328 hours will need at least 4.65 kWh of capacity at start of operation. This would provide for communications to operate on a 3% duty cycle throughout the lunar night. A 100-hour duration will require 1.4 kWh of capacity at start of operation in this configuration. These numbers are preliminary estimates. Actual pack sizes and operational temperatures are calculated in later sections.

The battery will provide 28 volts in an 8s configuration (8 cells in series). The following equation was used to calculate the required number of cells per pack:

$$N_P = \frac{C_p V_c}{C_c V_p}$$
(2.1)

Np is the number of cells in the pack, C_p is the required pack capacity in Whr, C_c is the cell capacity in Ahr, V_c is the nominal cell voltage in volts, and V_p is the required pack voltage. A representative lithium-ion cell has a capacity of 3.5 A-hr., a nominal operating voltage of 3.6 volts, and weighs 50 g.   A pack designed to last the night at the equator would require 376 cells, weigh 21 kg, and occupy 1.14 m³. This assumes 10% growth in mass for the battery structure and 30% growth in volume due to structure and insulation. A pack designed for the south pole would require 112 cells, weigh 6 kg, and occupy 0.34 m³. As can be seen later, the pack sizes are increased when heaters are added for night-time operational temperature control.

2.2   Communications Model

For mid and low latitude installations, the Earth and orbiting satellites will always be in view of the communications station. Ground based optical communications stations are in Table Mountain in California (117.7° W) and Waimea Hawaii (155.5° W) and will likely be installed on the International Space Station soon. RF communication options are in Goldstone in California (116.8 W), Madrid in Spain (3.1° W), Canberra in Australia (149.0° E), and the ISS. Assuming that optical communication is unreliable when the ground station is less than 20° from the horizon due to atmospheric interference, the ground station has a 50° window of operation. The California and Hawaii installations are within 50° of each other, this results in coverage between 92.7° and 180.5°, or about six hours in every 24-hour period. The ISS orbits the Earth roughly every 90 minutes. Assuming the station is in line of sight for roughly half the time, this results in 45 minutes of coverage every 90 minutes. This coverage is likely similar for other laser communications satellites such as LCRD.

For installations at the south pole, line of sight with the Earth will be lost every 14 days requiring all communications to be conducted with satellites orbiting the moon. Primary candidates are the Lunar Reconnaissance Orbiter (LRO) and the lunar gateway. The LRO is already well past its original mission life.   The LRO is in a 50km polar orbit with a period of 113 minutes [20]. It will be assumed that installations at the south pole will be visible to the LRO for 25% of its orbit period, or 28.25 minutes every 113 minutes. The Lunar Gateway will operate in a near rectilinear halo orbit. Using the CAPSTONE demonstration mission as a baseline for this orbit, we will assume an orbital period of approximately 7 days, and perigee and

apogee of 3,500 and 70,000 km respectively [35]. With this orbit, the Gateway will be in view of the south pole approximately 96.3% of the time, or 9,712 minutes in every 10080 minutes.

2.3   Power Model

Power is consumed from a variety of sources. If all subsystems are active simultaneously, the power draw is 145.2 W. Not all subsystems will be active all the time, but it is conceivable there will be situations where all are active. It will be assumed that communications systems will be active 80% of the time during windows when communication is possible. The solar panels are sized such that the system will be able to fully charge even if all systems are consuming full power. Later, when the output of the solar panels decreases due to dust, the duty cycle during daylight hours could be reduced.

If the minimum number of subsystems are active (heaters not included), the power draw is 7.2 W. In this configuration, the system operates in a low-power mode. Communications systems may be used but shouldn't exceed 1577 W-hr. at the equator or 481 W hr. at the poles. This amounts to a 3.15% duty cycle for the optical communications system, or 26.7% duty cycle for the s-band comms. A full breakdown of the subsystems and their respective power draw are shown in the table below.

It is assumed the system will be installed during daylight hours and the system will first have to survive the lunar night before starting operation. It will begin its mission at the start of the following day with 20% battery capacity remaining.

Table 2.2 - Subsystem power requirements

Component	Active Power [W]	Inactive Power [W]
PPM Modem	78	0
Optical Communications Module (x2)	24	0
RF Radio	18	0
Power Management System 1	10	0
Atomic Clock [27]	8.3	1.8
Camera	4.5	0
Logic Controller	1.3	1.3
GPS	1	0
SI-Audio Seismometer	0.1	0.1
Power Management System 2	0	4
Short-Period Seismometer	0	0
Total	**145.2**	**7.2**

2.4 Thermal Characterization

2.4.1 Energy Transfer Models

The thermal system is characterized by two primary driving phenomena: conduction and radiation. Because testing on Earth may also involve convection, it will be included in a separate analysis that can be used for comparison.

The driving equation for conductive heat flow is:

$$q_k = -Ak\frac{dT}{dx} \tag{2.2}$$

By integrating this equation over length L with respect to T and evaluating for temperatures T1 and T2, we get the following expression:

$$q_k = \frac{Ak}{T}(T_1 - T_2) \tag{2.3}$$

The driving equation for radiative heat transfer is:

$$q_r = \sigma A T^4 \tag{2.4}$$

This equation assumes the radiative surface is a perfect blackbody radiator. Real-life surfaces aren't generally blackbodies, though we will consider space to be a blackbody. When considering heat radiated from the equipment's surface into space, we will use the expression:

$$q_r = \sigma \varepsilon_1 A(T_1^4 - T_2^4) \tag{2.5}$$

For radiative heat transfer between the equipment and regolith on the lunar surface, the expression becomes:

$$q_r = \sigma \mathcal{F}_{1-2} A(T_1^4 - T_2^4) \tag{2.6}$$

$\mathcal{F}_{1-2}$ is the shape factor between the two surfaces. The expression used for convective heat transfer will be

$$q_c = \overline{h_c} A \Delta T \tag{2.7}$$

where ΔT is the difference between the surface temperature and the fluid.

CFD analysis will be completed using ANSYS Workbench. ODE solvers operate on the principle of conservation of mass, momentum, and energy. The solvers assume certain boundary conditions (Dirichlet and Neumann for example) and use time marching methods to iteratively solve for the solution. Depending on the analysis, the terms included in the set of equations may change. Since initial analysis won't include convection, the solution will be driven by the heat equation [33]:

$$\frac{\partial u}{\partial t} = v\left(\frac{\delta^2 u}{\delta x^2} + \frac{\delta^2 u}{\delta y^2} + \frac{\delta^2 u}{\delta x^2}\right) \tag{2.8}$$

When including convection, the equation becomes the linear convection-diffusion equation:

$$\frac{\partial u}{\partial t} + \alpha\left(\frac{\delta u}{dx} + \frac{\delta u}{\delta y} + \frac{\delta u}{\delta z}\right) = \nu\left(\frac{\delta^2 u}{\delta x^2} + \frac{\delta^2 u}{\delta y^2} + \frac{\delta^2 u}{\delta x^2}\right) \tag{2.9}$$

2.4.2 Mission Analysis and Approach

The system needs to be optimized to allow the operational limits for the various subsystems to be maintained. For a system that uses regolith as insulation, it is assumed the sub-surface temperature will be constant at -25°C and that components will have minimal shielding. For systems on the surface with designs that don't use regolith as insulation, the design will include surface coatings and insulating tape as a shield from radiative heat transfer. Components in contact with regolith will be designed to minimize conductive heat transfer.

Initial analysis will be performed using all available hardware operational and performance data. Estimates for electrical component generated heat will be made and included in a separate analysis. Once the initial analysis is complete, the design will be iterated, and heaters or heat pipes will be added as necessary.

Table 2.3 - Component operational temperature limits

Component	T_min [°C]	T_max [°C]
Battery Cells	0	45
Optical Comm Modem	0	40
Camera	0	30
PPM Modem (discharge)	-10	60
RF Radio	-20	60
Short-Period Seismometer	-20	20
Atomic Clock	-20	65
Logic Controller	-30	60
Power Management System 1	-30	60
Power Management System 2	-30	60
SI-Audio Seismometer	-35	75
GPS	-40	85
Optical Comm Module Actuator	-45	85

2.5 Battery Cell Considerations

If the battery is required to be installed as part of a crewed mission, the battery cells and pack will need to be subjected to testing to ensure the safety of the crew. Testing includes multiple charge/discharge cycles conducted after subjecting the pack to temperature and vibration conditioning. Batteries that are delivered to the surface by delivery vehicles that do not include crew are subject to much simpler test requirements and potentially cost less. In addition to the

conditioning and testing, the pack will be designed in such a way to minimize impact to its environment in the event of a catastrophic failure.

All sub-surface modules include a case around the battery with a gap between the battery and the case. The case serves two important functions. The size and number of structural supports and the surface emissivity can be tuned to keep sub-surface components within operational ranges. In the event of battery cell failure, the gap between the cell and the case will help contain fluids from leaking cells or flames in the event of thermal runaway. In addition to the case, cells will be potted using a flame-retarding material designed to prevent catastrophic damage to adjacent cells.

3. Communications and Power Simulation

3.1 Simulation Description

A MATLAB script was developed to analyze the various lines of sight for optical and RF communications using the results discussed in the Communications Model section above. Simulations were developed for both the equatorial and polar scenarios. If optical communications coverage was available, that was prioritized over RF communications as the data rate is higher. When solar power is available, the communications systems will run at 100% duty cycle, with optical communications prioritized over RF communications. During the night, the communications system runs on a 3% duty cycle for optical and up to 5% duty cycle for RF communications. Due to the complexity of analysis, equatorial communications analysis does not include the Lunar Gateway or the Lunar Reconnaissance Orbiter.

3.2 Simulation Results

3.2.1 Equatorial Results

Optical communications availability for a full lunar solar cycle (655.2 hours) is shown in the figure below. The number of visible stations is summed and represented as the "Total Optical Coverage" line. In the first 24 hours of the simulation there are periods as long as 45 minutes with no optical coverage. This occurs when the International Space Station is behind the Earth. RF coverage was analyzed the same way.
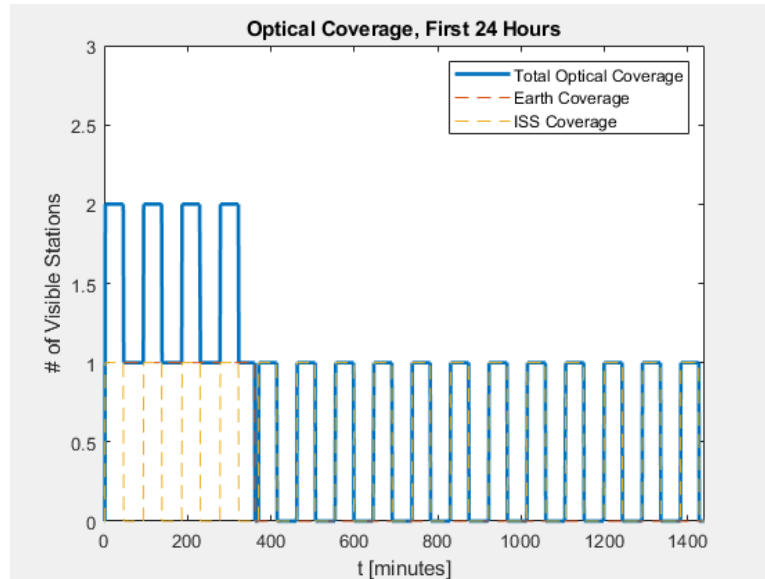
Figure 3.1 - Equatorial optical communications coverage analysis
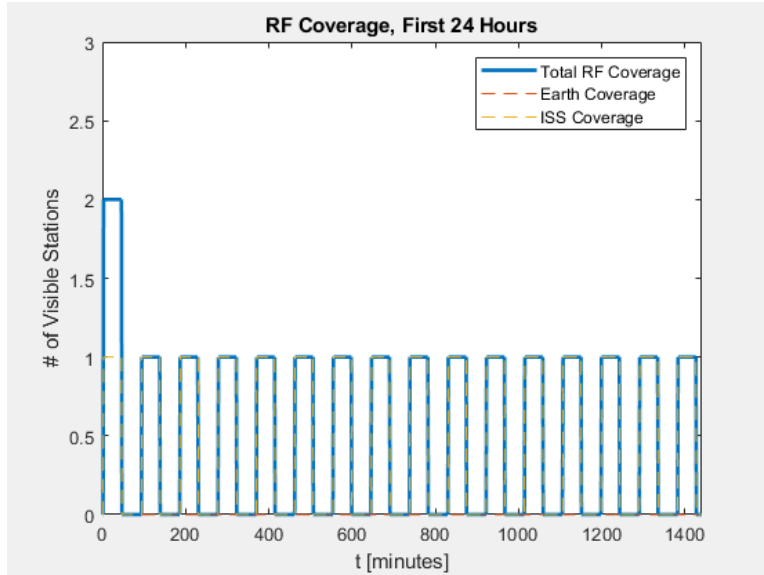
Figure 3.2 - Equatorial RF communications coverage analysis
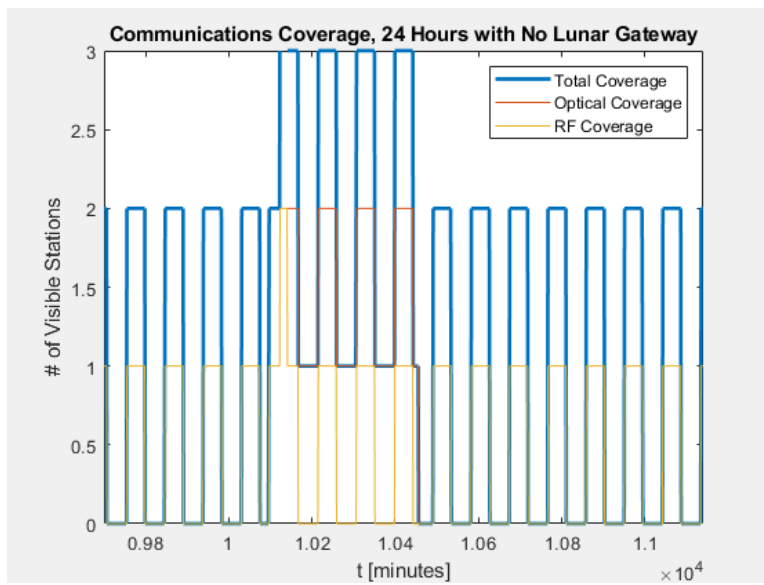
Figure 3.3 - Total communications coverage analysis with no Gateway

The solar panel is sized to allow the communications systems to run at 100% duty cycle while also charging the battery. When the battery is full, the system will maintain the battery at 100% state of charge. The battery state of charge and the total downlink data transmission over a lunar solar cycle is shown in the figure below.
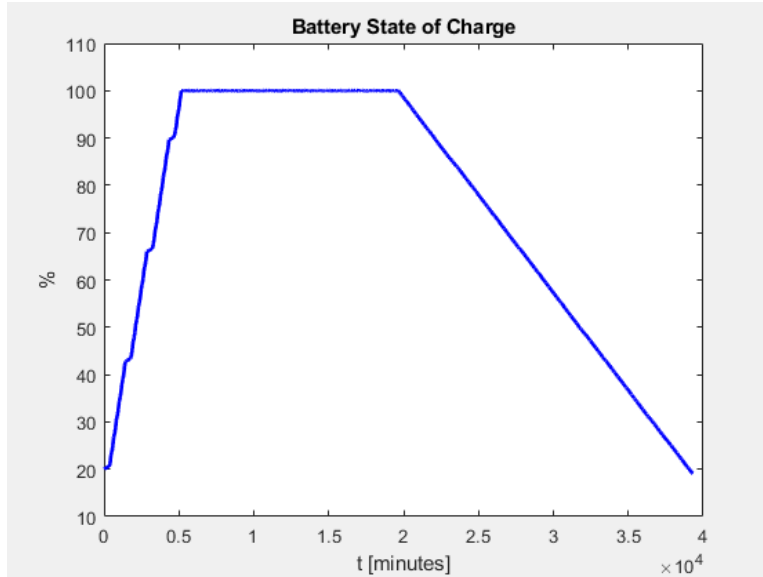
Figure 3.4 - Equator battery state of charge
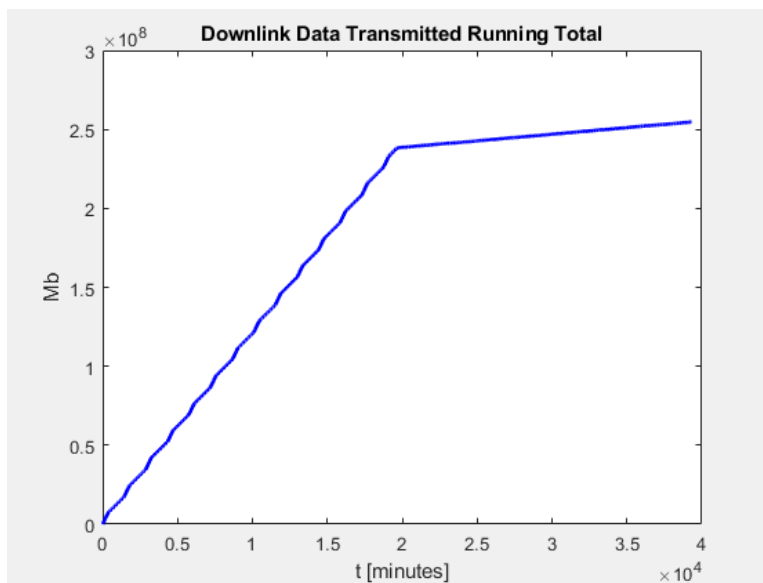
Figure 3.5 - Accumulated downlink data

3.2.2 Polar Results

Optical communications availability is shown in the figure below. In the first 24 hours of the simulation there is always coverage. RF coverage was analyzed the same way, in the first 24 hours there is always coverage. While there are a variety of sources, the most persistent source of communications coverage comes from the Lunar Gateway because of its near rectilinear orbit. When Gateway is behind the Moon, there are periods, some as long as 45 minutes, where there is neither optical nor RF coverage.
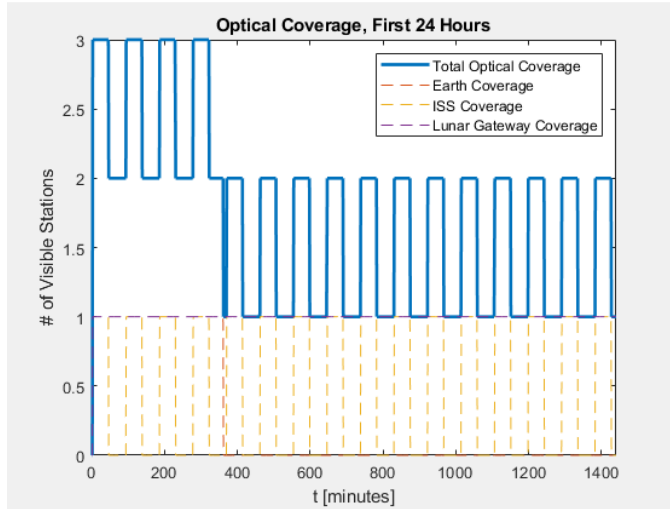
Figure 3.6 - Polar optical communications coverage analysis
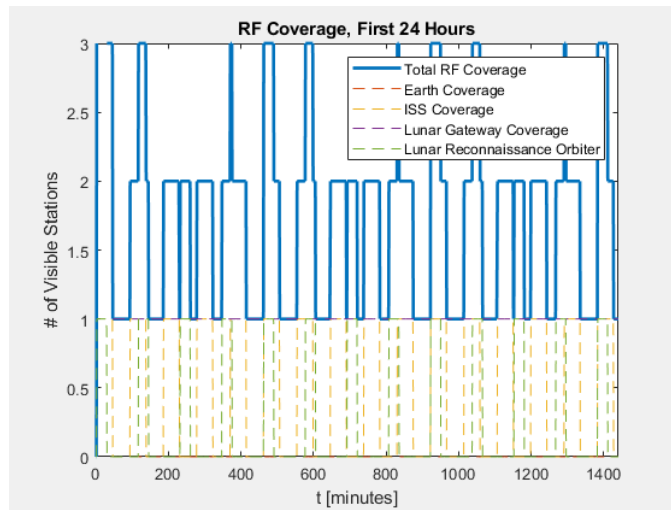
Figure 3.7 - Polar RF communications coverage analysis
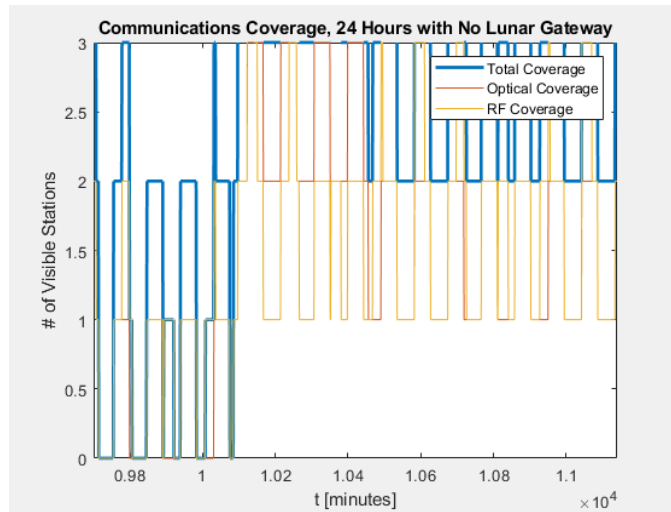
Figure 3.8 - Total communications coverage analysis

The battery state of charge and the total downlink data transmission over a lunar solar cycle is shown in the figure below.
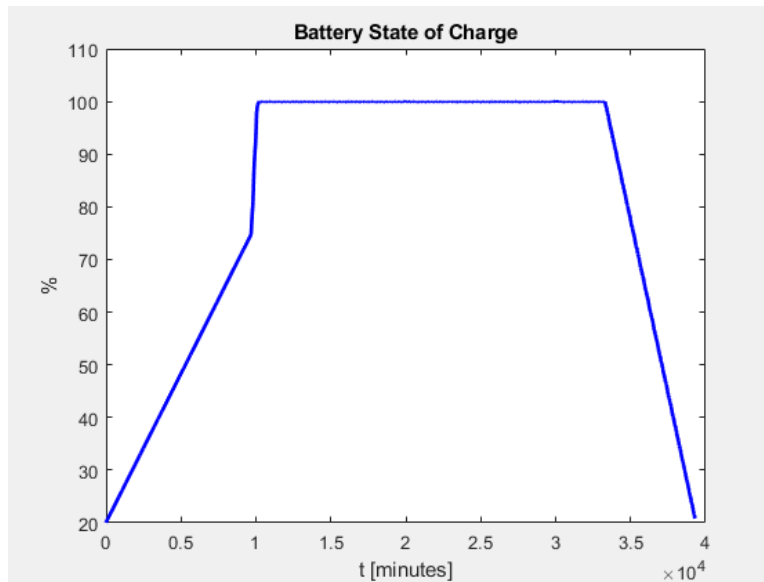
Figure 3.9 - Polar battery state of charge
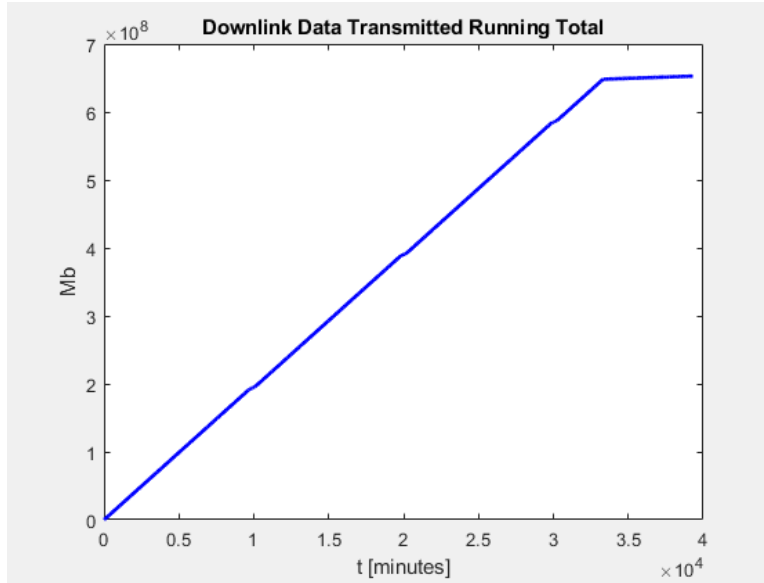
Figure 3.10 - Accumulated downlink data

4. CAD Model

4.1   Preliminary CAD Models

A CAD model was developed using the sizes and masses defined in the sections above. Components with similar thermal requirements were grouped together. The modem for the laser communications system was grouped with the lithium-ion battery. The seismometers were grouped with the battery as well to improve their contact with the regolith. RF and GPS antennas were mounted on the solar panel. A box was created to house all the other components apart from the camera. See the figures below.
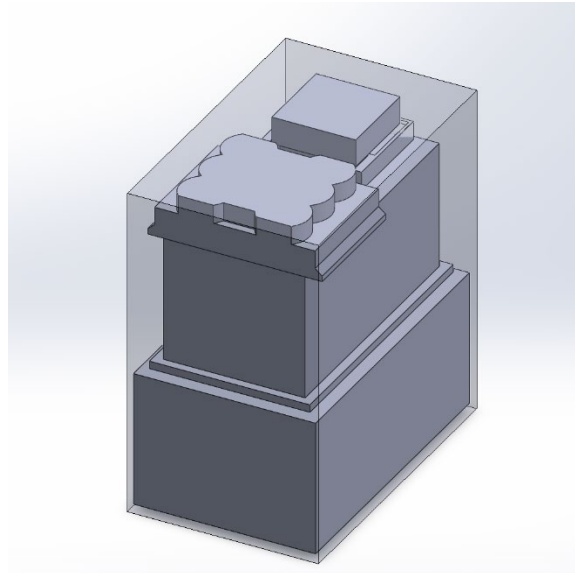
Figure 4.1 - Controller, atomic clock, radio, and power electronics
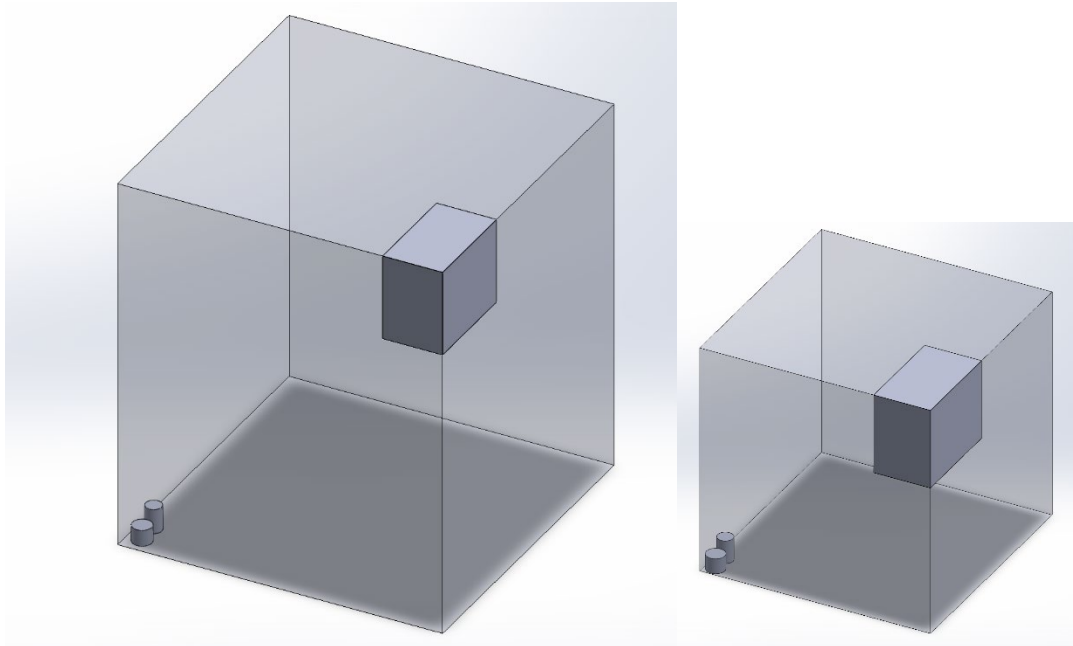
Figure 4.2 - Equator (left) and polar (right) batteries with optical modem and seismometers

4.1.1 Equator Model

In the equator model, the solar panel is mounted horizontally, and the optical unit and the imager camera are all pointed up. This configuration is conceivably the worst-case scenario from a dust accumulation standpoint.
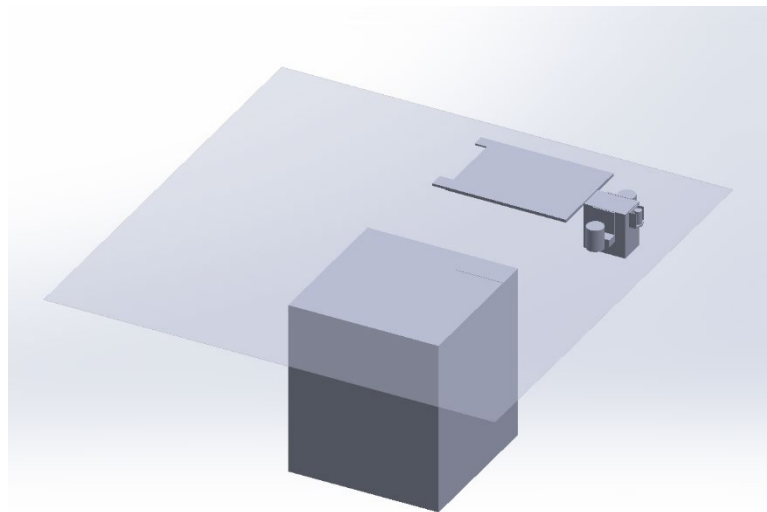
Figure 4.3 - Equator installation with sub-surface installed battery
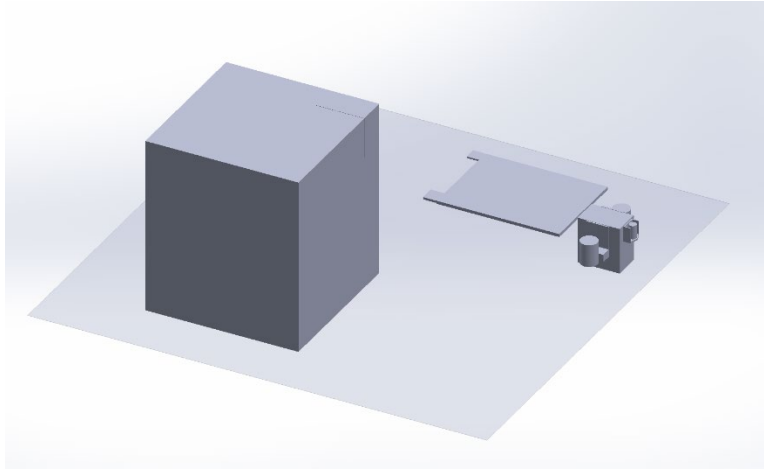
Figure 4.4 - Equator installation with surface-installed battery

4.1.2 Polar Model

In the polar model, the solar panel is mounted vertically with the optical unit and the imager camera horizontally. This configuration is conceivably the best-case scenario from a dust accumulation standpoint.
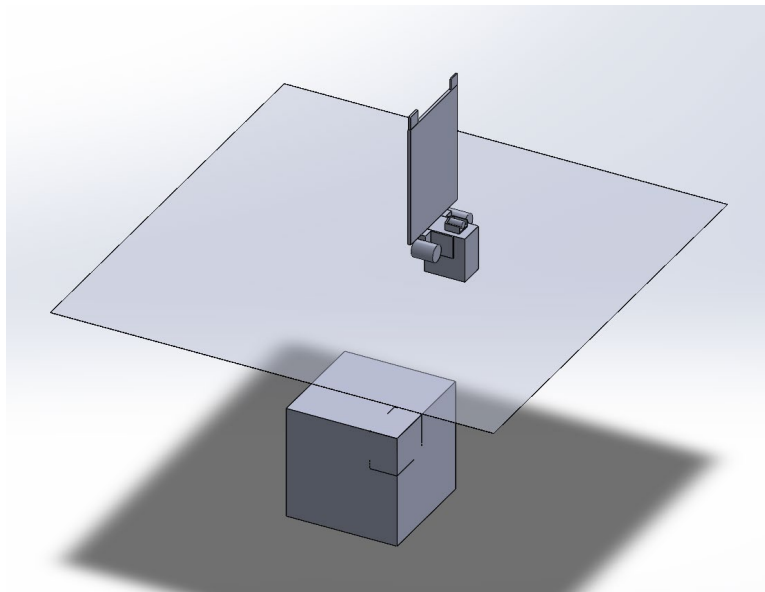
Figure 4.5 - Polar installation with subsurface battery
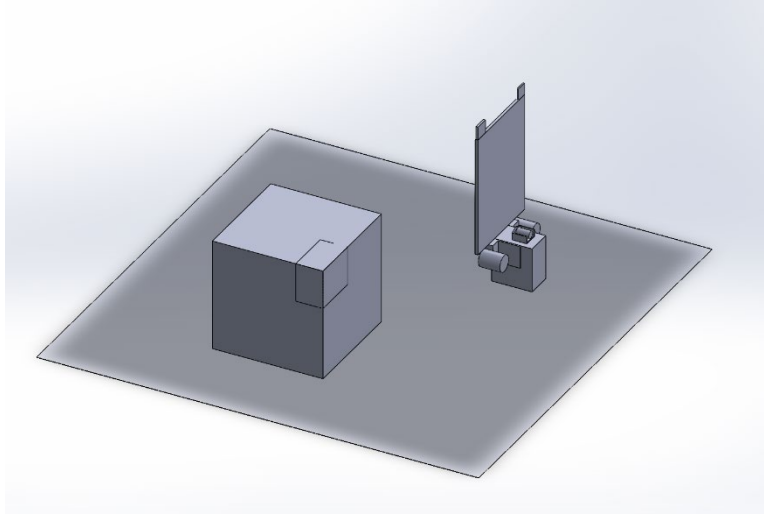
Figure 4.6 - Polar installation with surface-installed battery

5. Thermal Analysis

5.1 Thermal Model

The thermal model consists of a simplified representation of the fully developed solution. This allows for analysis of the bulk thermal behavior and gives a first approximation of the temperatures that can be expected. Most model components use cuboid shapes including the battery, electrical enclosures, optical modules, and solar panels. Supports and cable runs use cylinders. The tower uses solid square trusses with no joints. See figures below.
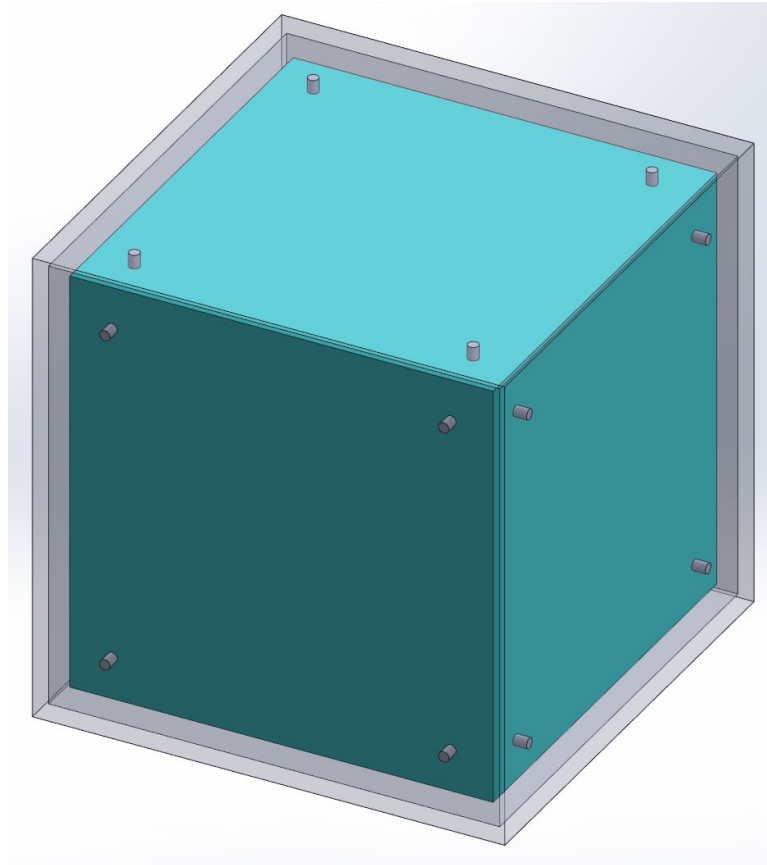
Figure 5.1– Battery module geometry for TC2

The regolith for sub-surface test configurations is split into two parts. This allows the temperature of the regolith at 1 meter depth to be held at a constant -25° C without having to model heat flux from the lunar core. A cavity the same size as the battery / electronics case is included just below the parting line. The regolith is extended far in the horizontal planes to minimize errors introduced from these boundary conditions.
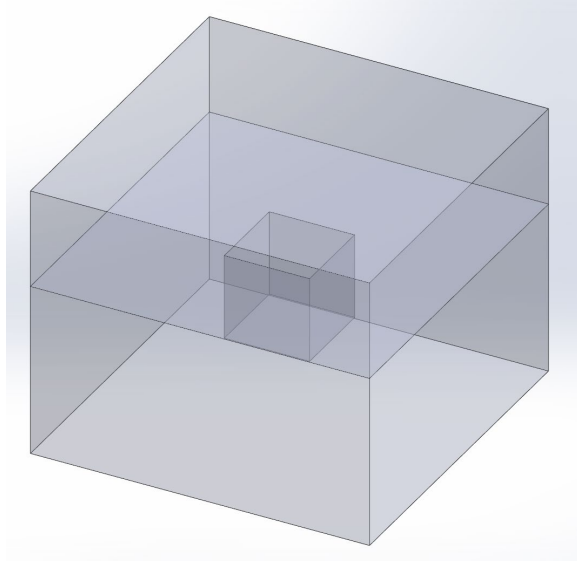
Figure 5.2 – Regolith geometry for TC2

Each test configuration includes a 1.6-meter tower that is used to mount the optical modules, solar panels, and other components as applicable. The tower will elevate the solar panels, increasing the duration that the panels receive light and providing some distance from the dusty regolith. The tower is designed to hold the solar panels at a 6° angle which will allow it to function with maximum efficiency. Panels for radiative heat rejection are installed on the tower above the solar panels. For TC3 and TC6, the case for the battery also serves as the radiator. There is approximately 2.5 m^2 of radiative area for each of the models.
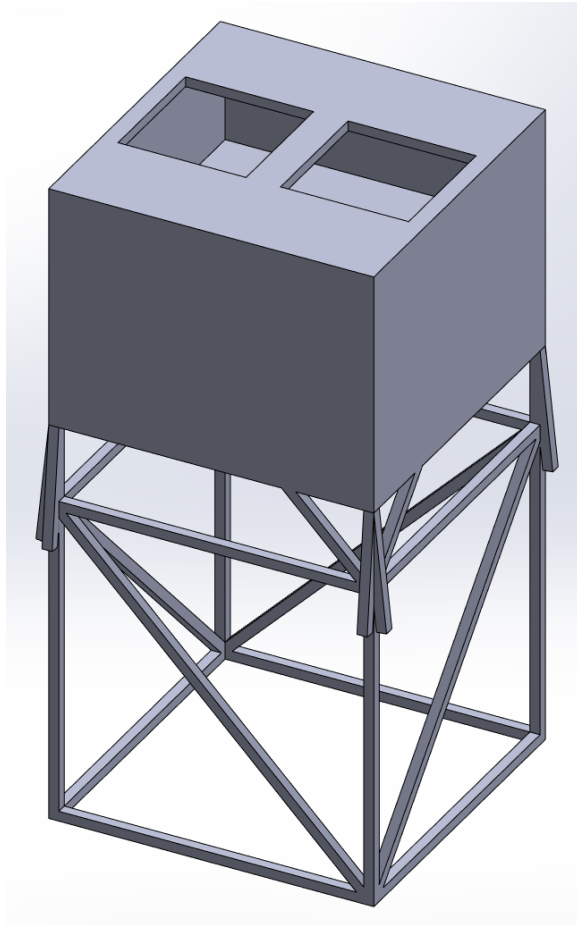
Figure 5.3 – Tower and thermal radiator geometry for TC2

Optical modules are mounted to the top of the tower. Like the battery, the optical module has an outer case, this one is made from glass. The optical module is supported by four supports with low thermal conductivity.
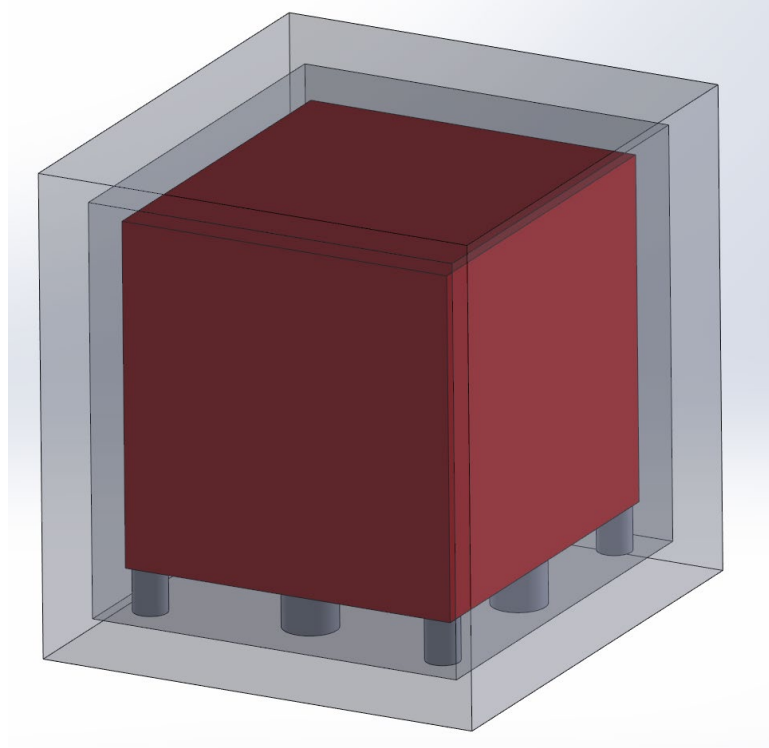
Figure 5.4 – Optical module geometry for TC1

There are thermal switches that connect the optical module, electronics module, and battery (as applicable) to the outer case. During nighttime, the thermal switches open to protect the modules from the cold surface temperatures. During daytime, the thermal switches close and allow the heat generated from the modules to be conducted to the tower and radiated to space. The number of thermal switches per test configuration varies depending on the amount of heat that needs to be conducted. In the analysis, the connection between the thermal switch and the enclosure was suppressed for nighttime analysis and unsuppressed for daytime analysis to simulate the on/off functionality.
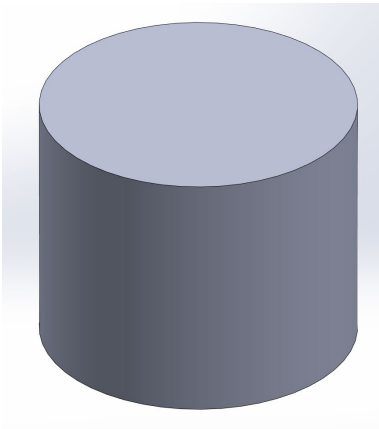
Figure 5.5 – Thermal switch geometry

5.2   Mesh

Meshing was completed using a 0.04 m (4 cm) element size. At this mesh size, the analysis included 240,734 nodes and 178,545 elements (TC1). This was the minimum size that would solve for both the thin walls of the enclosures as well as the large regolith volumes. Adaptive sizing was enabled. In order to maximize the accuracy of the model, the minimum wall thickness in the designs was no smaller than 25 mm. Results were compared to analysis using a 0.05 m element size and found to be converged as the variation between component temperatures was less than 1%.
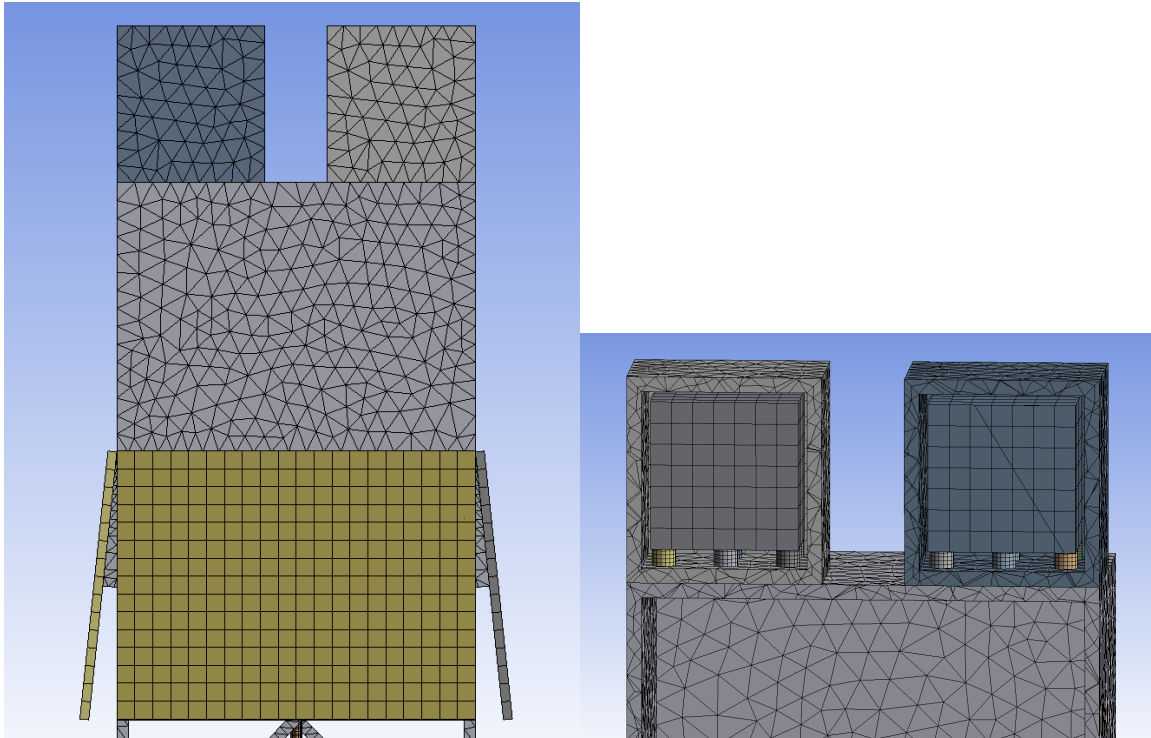
Figure 5.6 – Mesh using 4cm element size

5.3   Test Configurations

Analysis will be conducted on three test configurations for polar installation locations and three for equatorial locations for a total of 6 test configurations. Each test configuration will require different heating power to maintain hardware operating temperatures. Each configuration will have unique geometry.

The analysis approach was to first collect individual component power requirements as discussed in sections 1 and 2. A MATLAB simulation analyzes the per-minute power draw of each component over a full lunar day/night cycle (27.3 hours). The analysis outputs a surface and subsurface average power draw over day and night periods. This power draw was input as internal heat generation for the applicable components in the thermal model and the analysis was run with these numbers as initial values. If the temperature of the components fell outside of

operational ranges, the model was modified until operational ranges were achieved. For example, the internal heat generation for sub-surface components was increased or the surface emissivity was modified. Once the analysis converged on a solution, the final internal heat generation numbers were pulled into a table where the respective heating was calculated.

The strategy for the first configuration is to cover as much hardware as possible with regolith, insulating it from the temperature swings on the surface. In this scenario, the heat generated by the components during normal operation would be sufficient to keep all sub-surface hardware within minimum operational ranges during lunar day and night. The optical modules will require heating during cold hours, and thermal switches and radiators to keep them cool during hot hours. Because regolith is a good thermal insulator, heat is piped to the tower on the surface using four large heat pipes. For the south pole configuration, solar panels are mounted around the tower perimeter to accommodate 360° sunlight conditions. The batteries for all polar models measure 1 cubic meter.
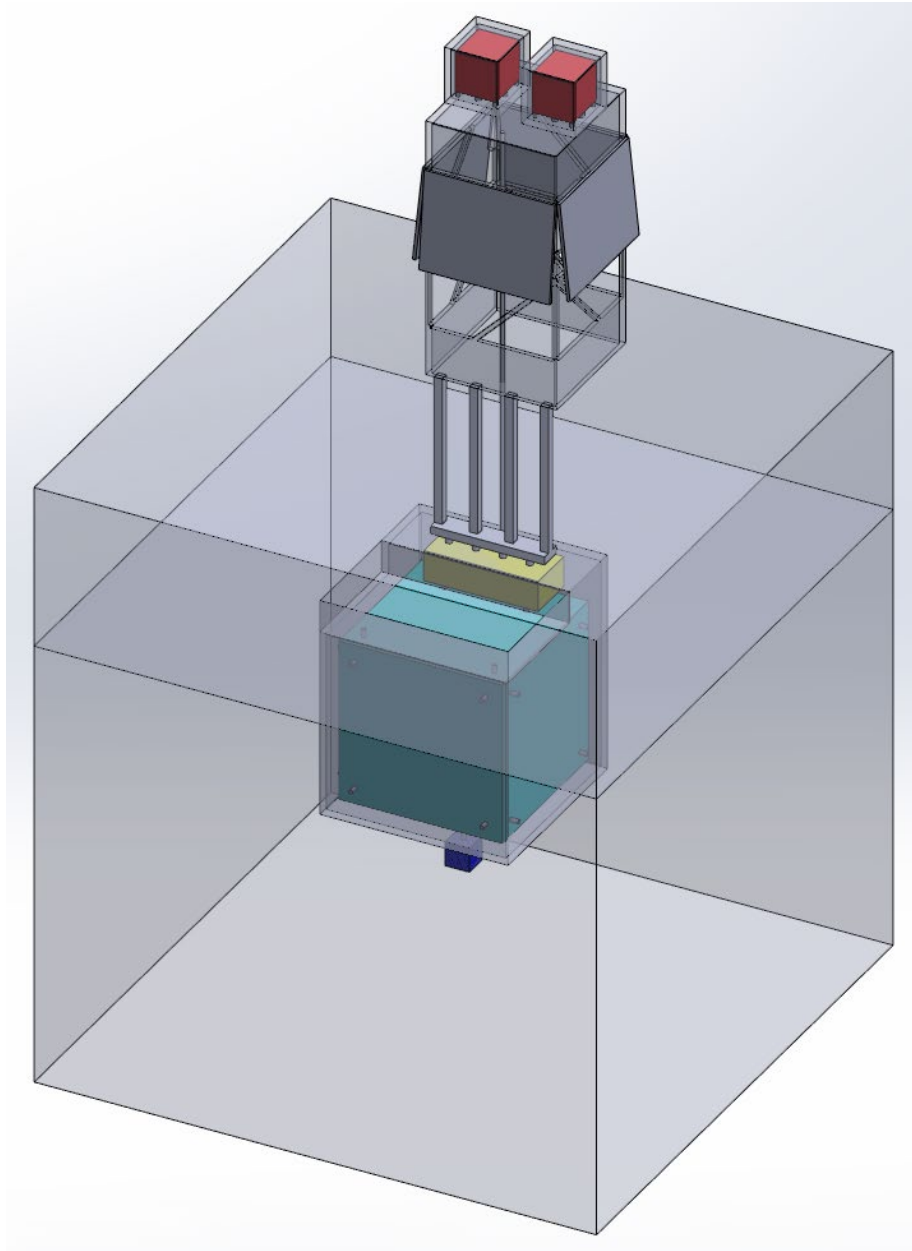
Figure 5.7 – TC1 polar thermal model

The second configuration considers placing only the battery under the regolith, mounting all other components to the tower. Here, the battery would require heating to charge it during lunar day and the electronics would require heating during the lunar night.
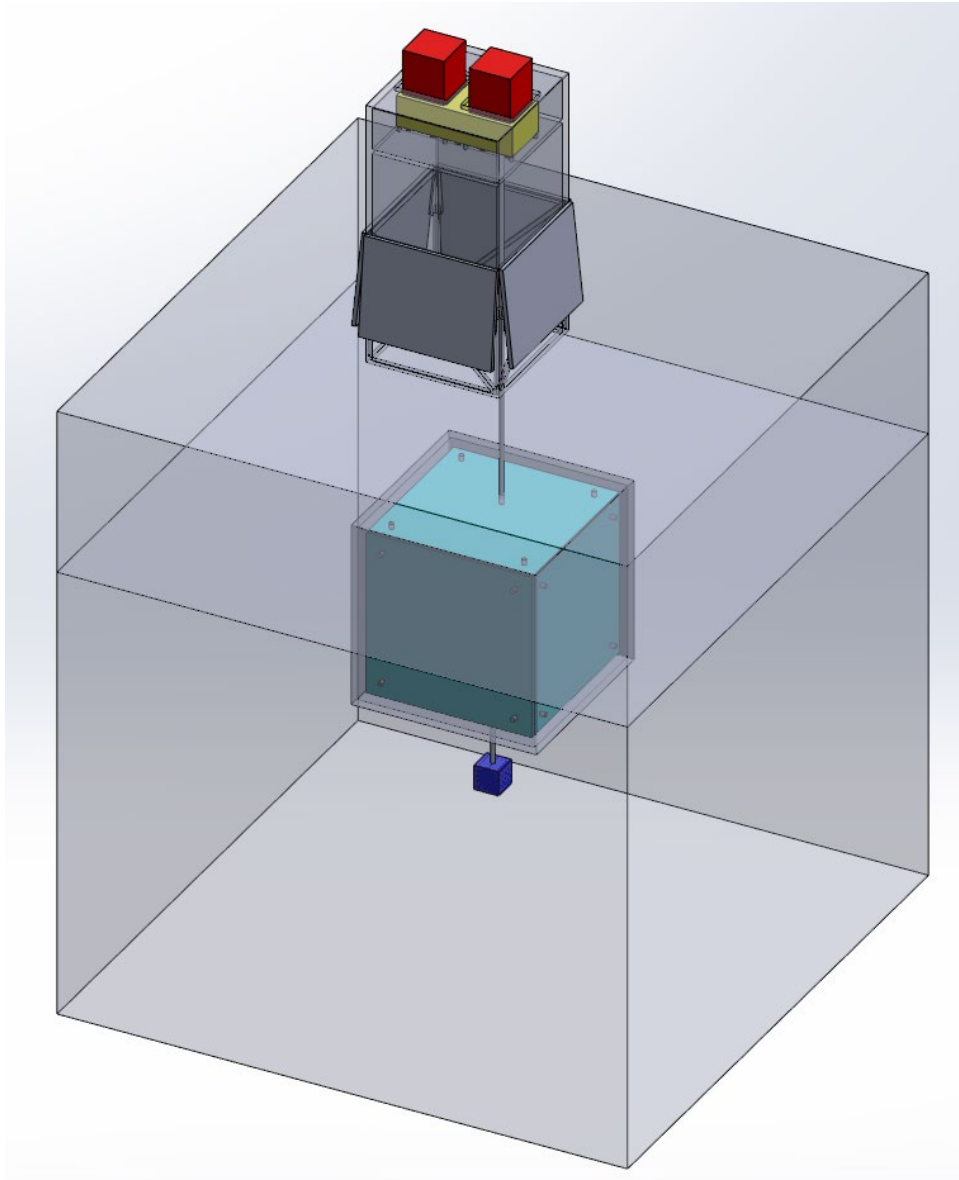
Figure 5.8 – TC2 polar thermal model

The third configuration considers mounting all components apart from the seismometers to the tower. Here, the battery and the electronics would require heating during the night.
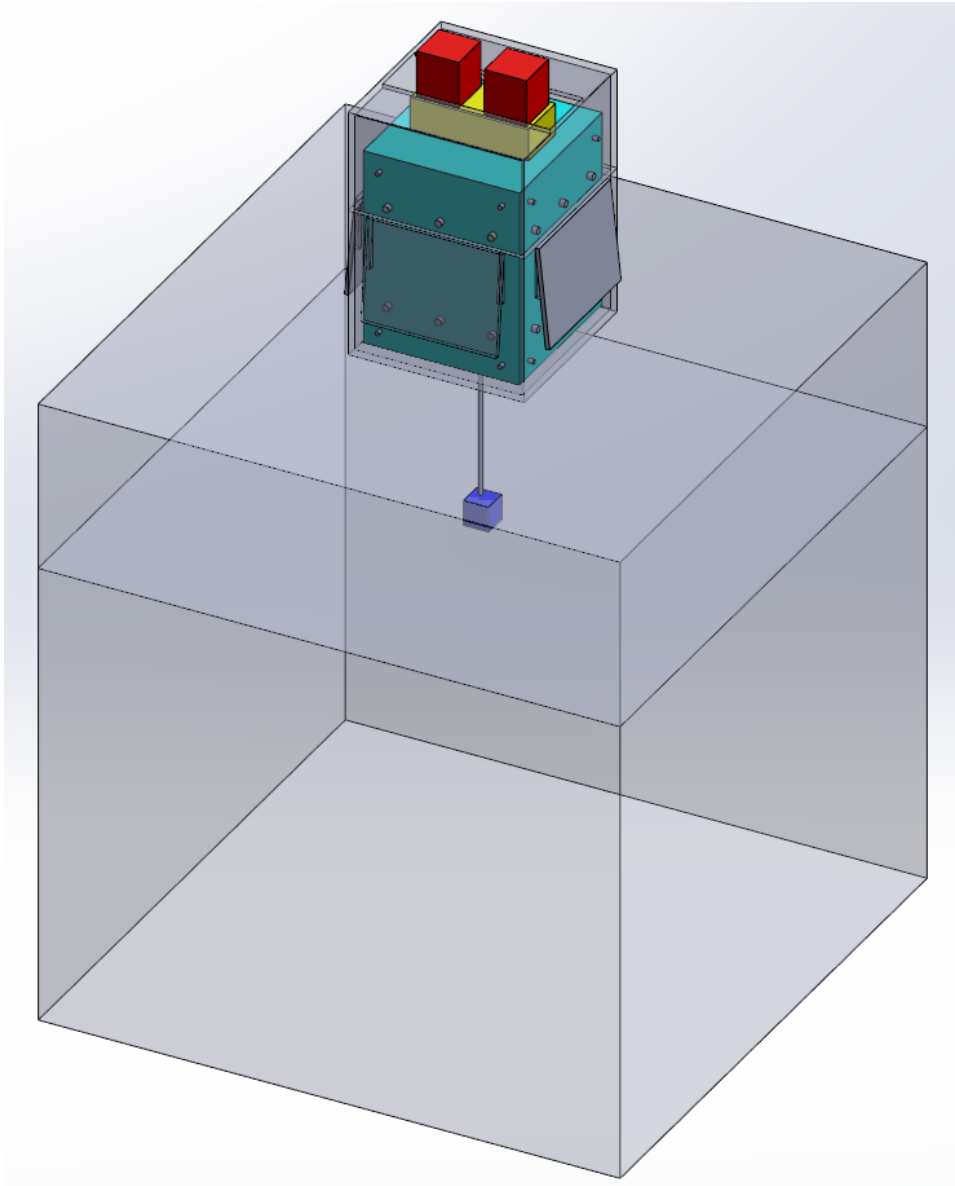
Figure 5.9 – TC3 polar thermal model

The thermal models for TC4, TC5, and TC6 mimic the configuration of the previous test configurations but with a larger battery required for the equator. Solar panels are mounted to the top and two sides so that solar energy is captured from sunrise to sunset. The batteries are cubes measuring 1.6 meters on a side.
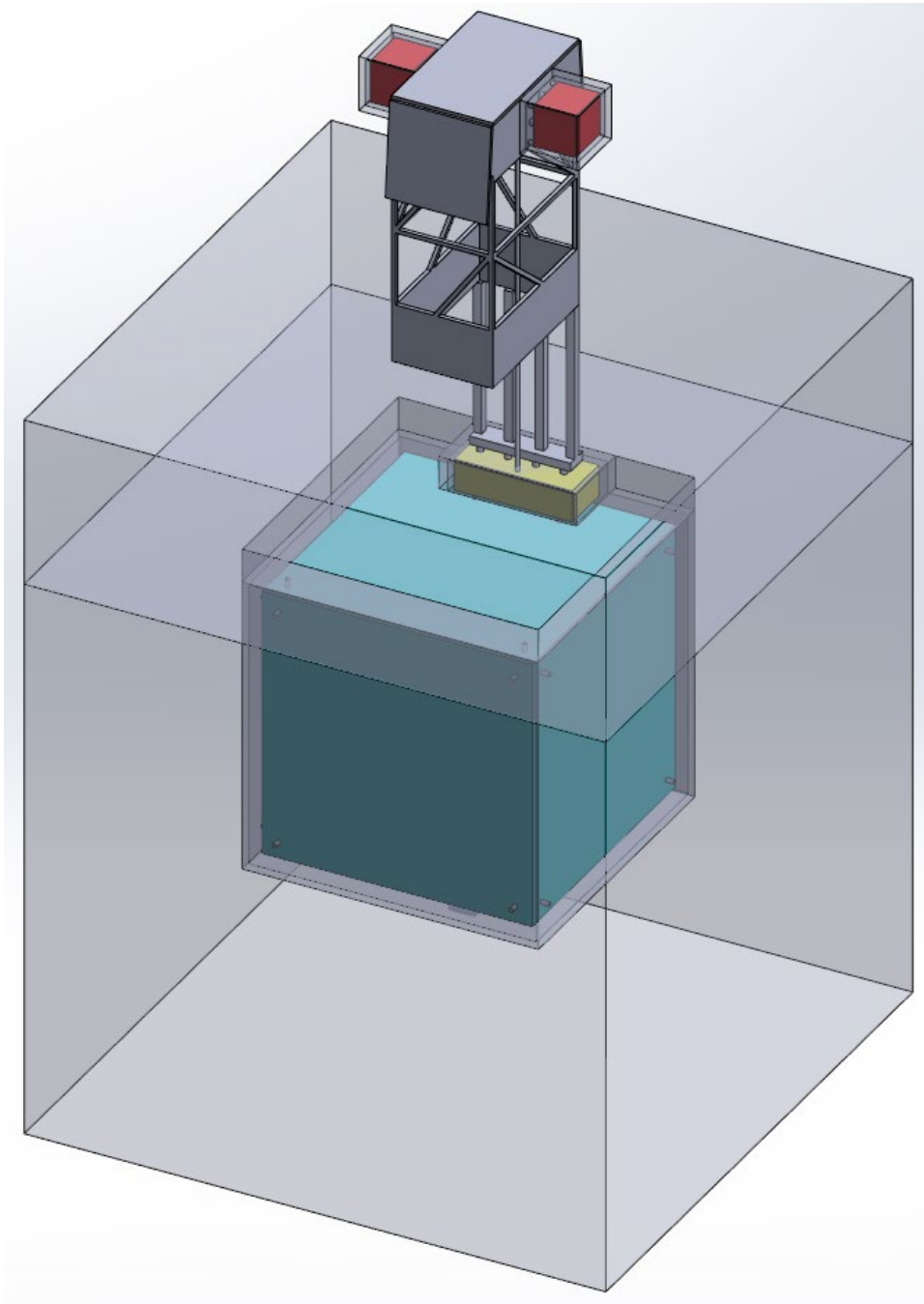
Figure 5.10 – TC4 equator thermal model
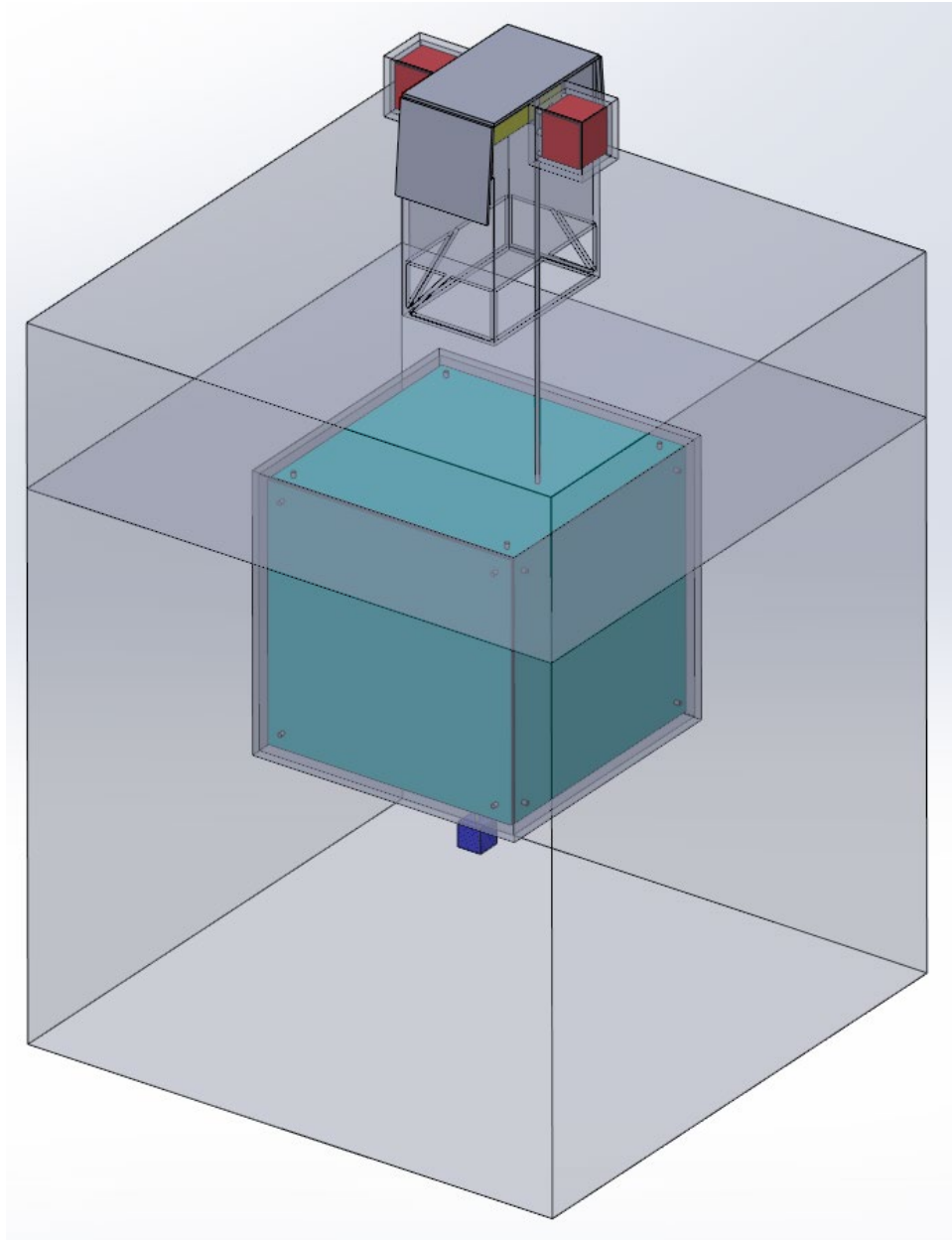
Figure 5.11 – TC5 equator thermal model
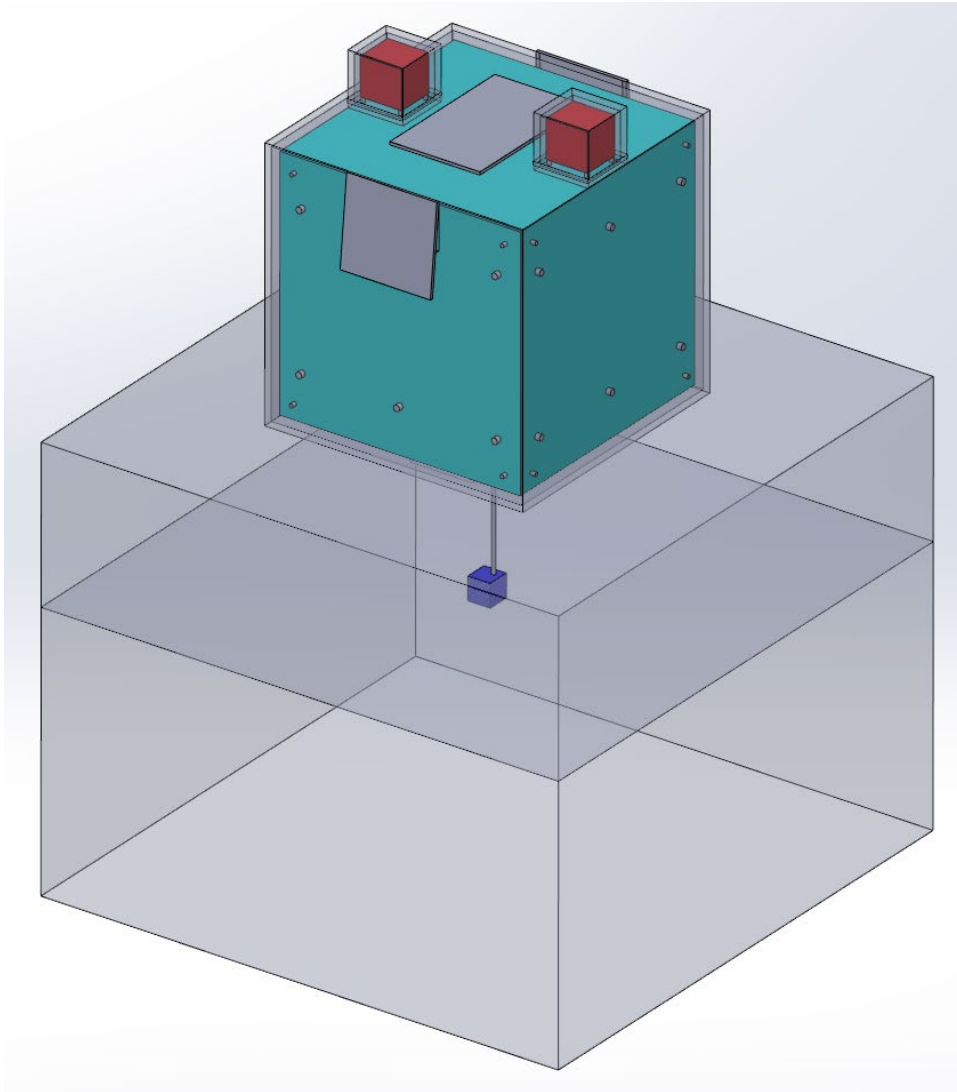
Figure 5.12– TC6 equator thermal model

5.4 Polar Analysis Results

5.4.1 TC1

Below are the boundary conditions for the first test configuration. Heat is transferred from the battery to the battery enclosure by conduction across thin polyethylene supports and by radiation. Heat from the optics module is transferred to the glass optics module covers across thin polyethylene supports, thermal switches, and radiation. Heat is conducted from the electronics module to the surface by four large heat pipes and by the power / data conduit. The conduction is turned off at night using thermal switches. Heat from the electronics module and the optics module are radiated using thermal radiators on the tower exterior. Solar flux is present during daytime analysis. Surface and subsurface temperatures are defined by measurements discussed in earlier sections of this report. Heat is generated inside component volumes including the battery, seismometer, electronics module, and optical module as needed to maintain minimum operating temperatures.
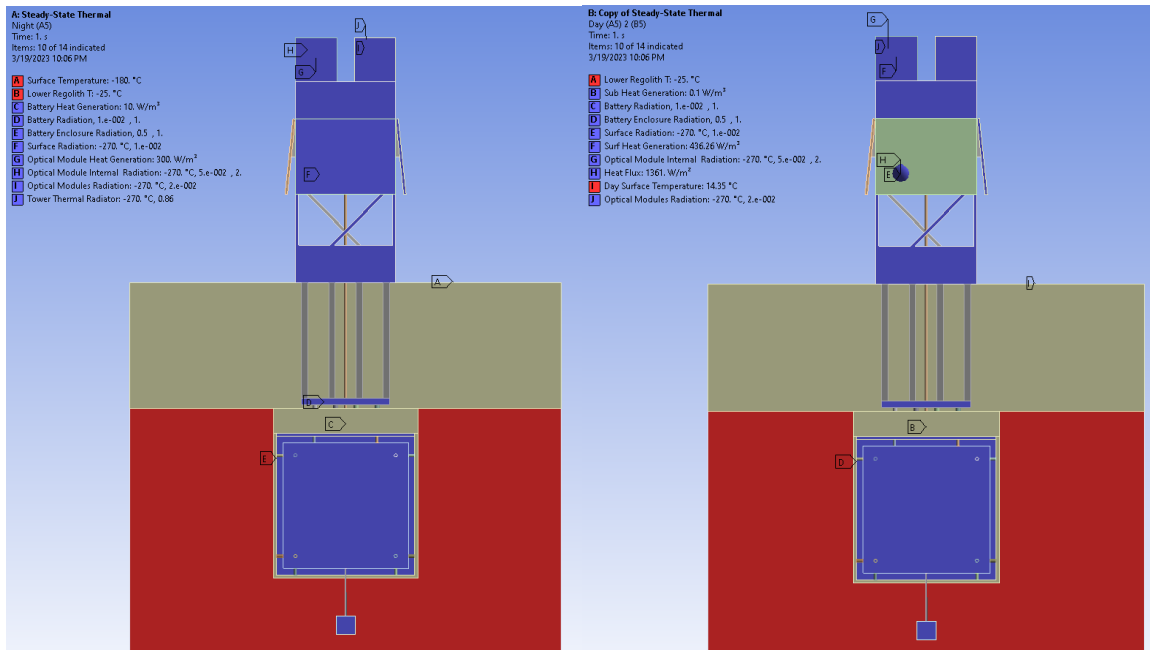
Figure 5.13 – Night (left) and day (right) boundary conditions for TC1

During nighttime hours, the tower temperature is dominated by the cold surface temperatures. Operation of the optical communications system provides some of the heating needed to maintain operational temperatures, but heaters are also required. The power generated by the electronics module (primarily the optical communications modem) heats the battery and seismometer while thermal switches isolate the components from the tower. As the battery and electronics must be isolated from the cold surface temperatures (and thermal control is achieved using passive systems), close attention must be paid to the maximum subsurface temperatures.
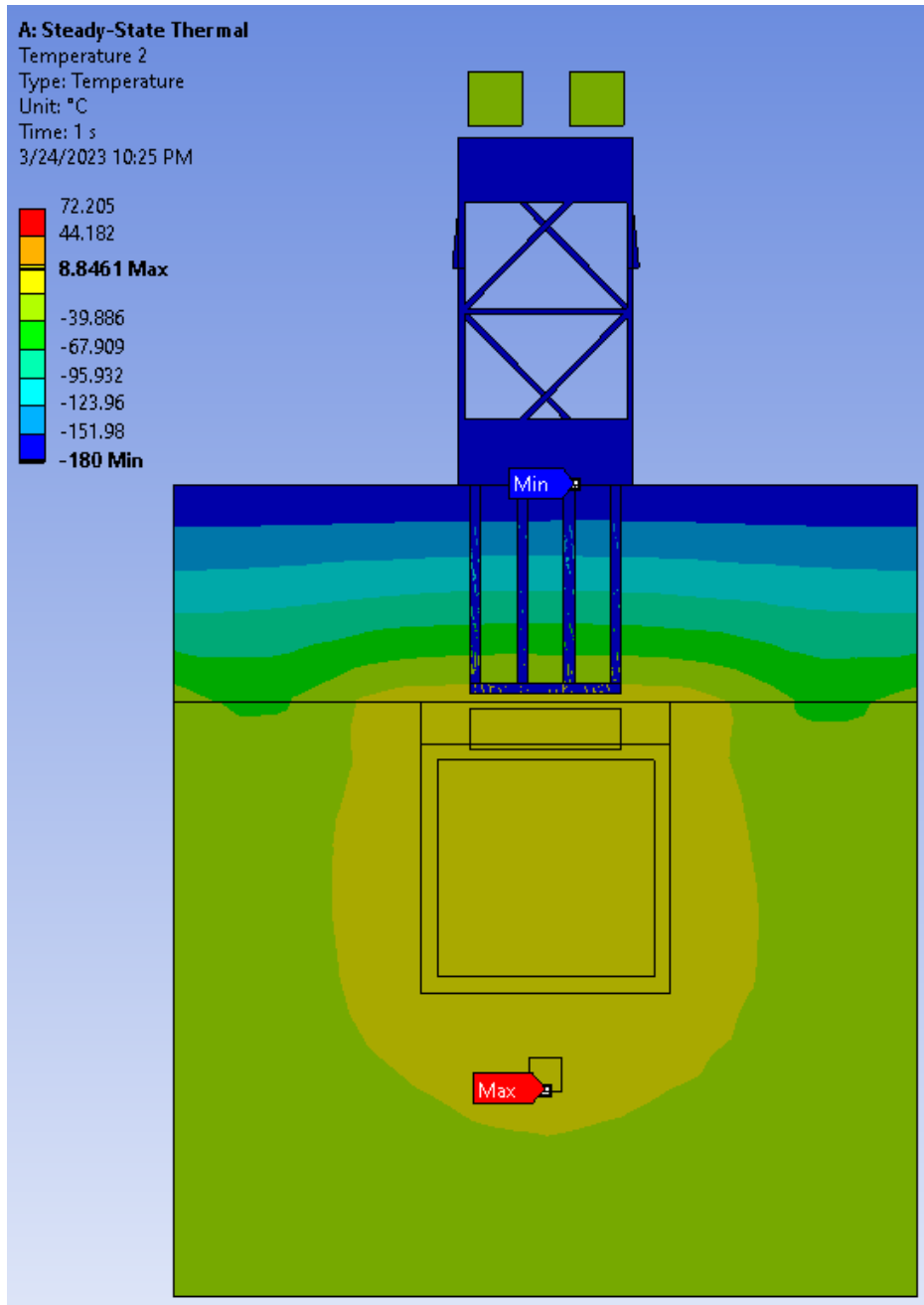
Figure 5.14– Nighttime battery, electronics, and optical module temperatures for TC1

During daytime hours the optical communications system more active, generating more heat. The thermal radiators (placed at both the tower top and bottom for TC1 and TC4) are crucial to maintaining operational temperatures. The glass covers provide some measure of protection to the optical modules and the thermal switches conduct heat generated by the components to the tower. Thermal switches also play a crucial role in conducting heat from the electronics module

to the heat pipes and thermal radiators. The solar panels provide some measure of protection from the solar fluxes reducing the heat flux to the tower.
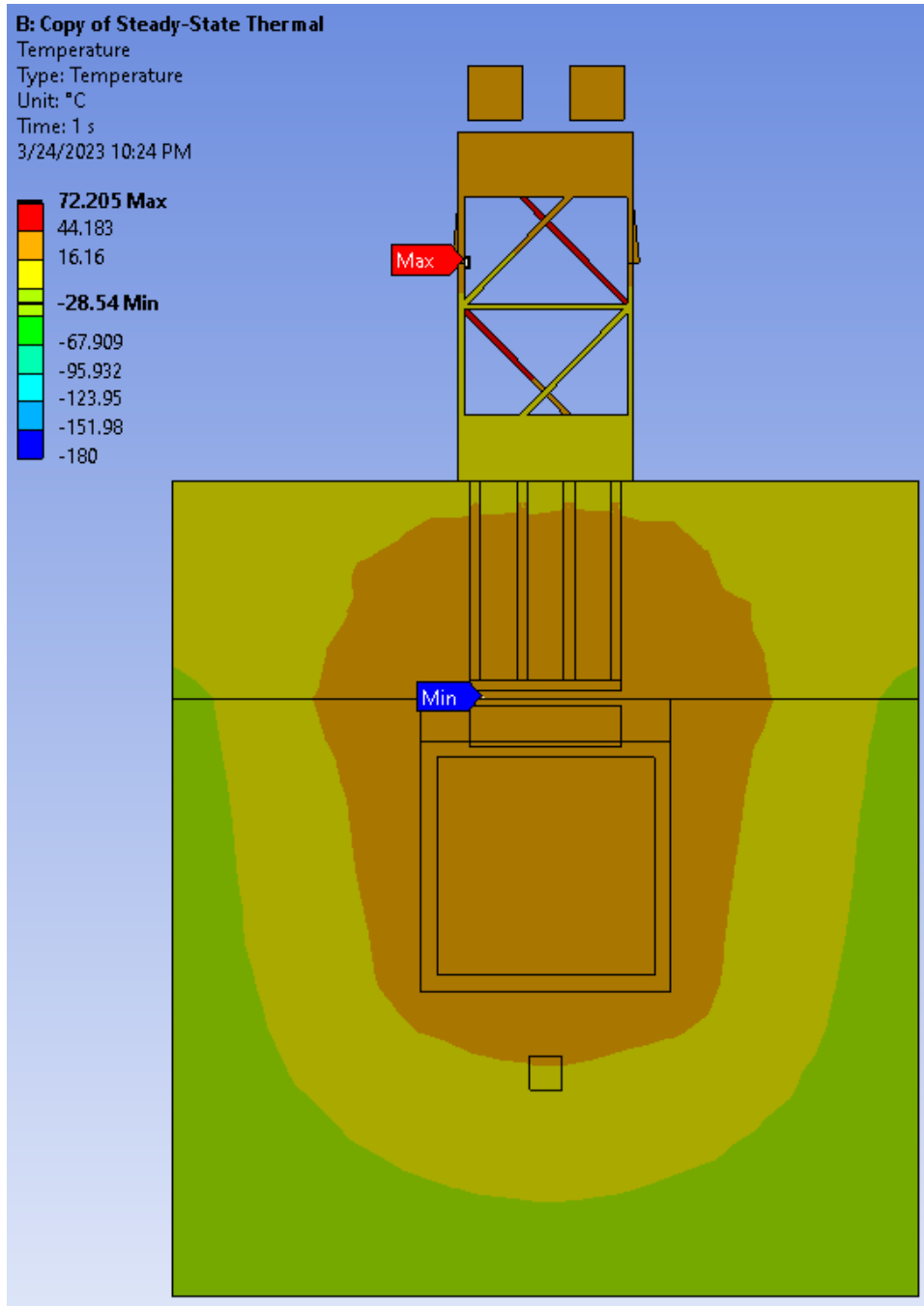
Figure 5.15 – Daytime battery, electronics, and optical module temperatures for TC1

The boundary conditions for TC2 are similar to TC1 with the exception of glass covers for the optical modules. These are in direct thermal conduct with the (top mounted) electronics module which is mounted to the tower using thin polyethylene supports and thermal switches.

Thermal radiators surround the electronics module and extend down for half the height of the tower. Solar panels are mounted around the bottom half of the tower.

5.4.2 TC2
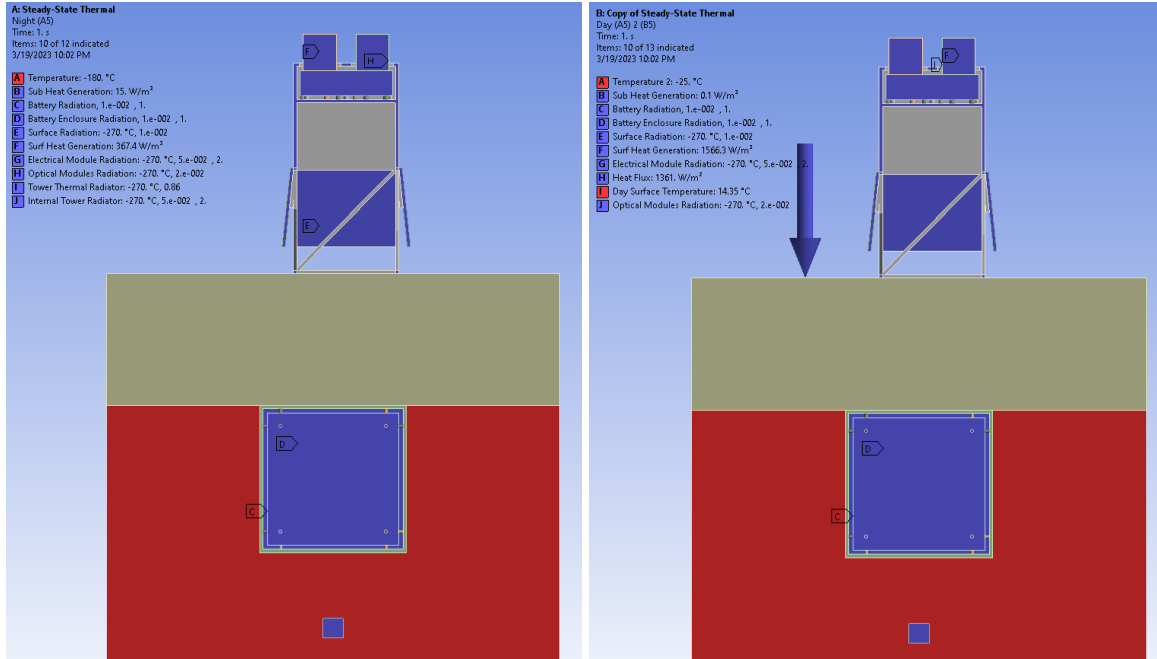
Figure 5.16 – Night (left) and day (right) boundary conditions for TC2

At night, heat from operating the optical communications system provides much of the heat needed to maintain operational temperatures above the surface. Some heating is required to maintain seismometer and battery minimum temperatures.
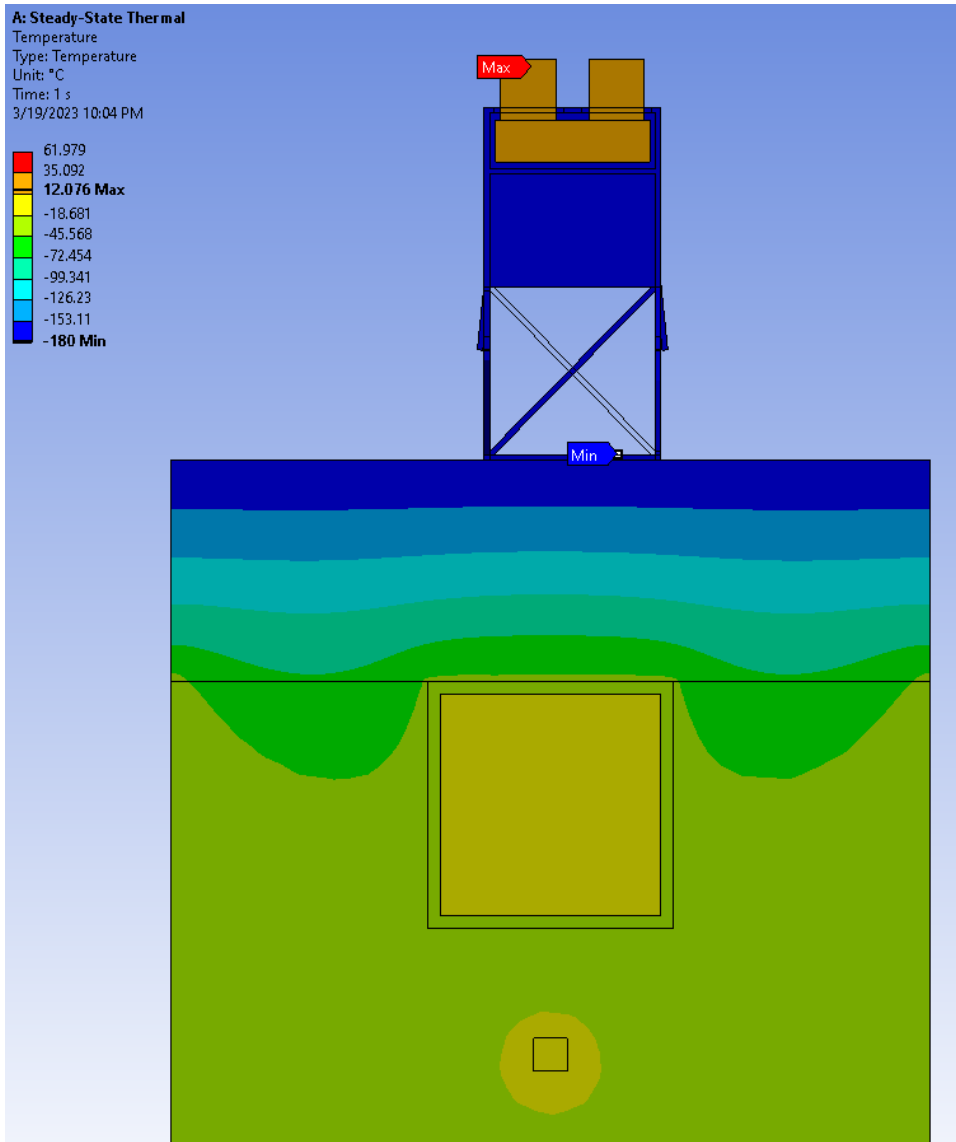
Figure 5.17 – Nighttime battery, electronics, and optical module temperatures for TC2

During daytime hours, heaters are all off and the primary challenge comes from rejecting the heat from operation of the communications systems and solar fluxes. A large thermal radiator is crucial.
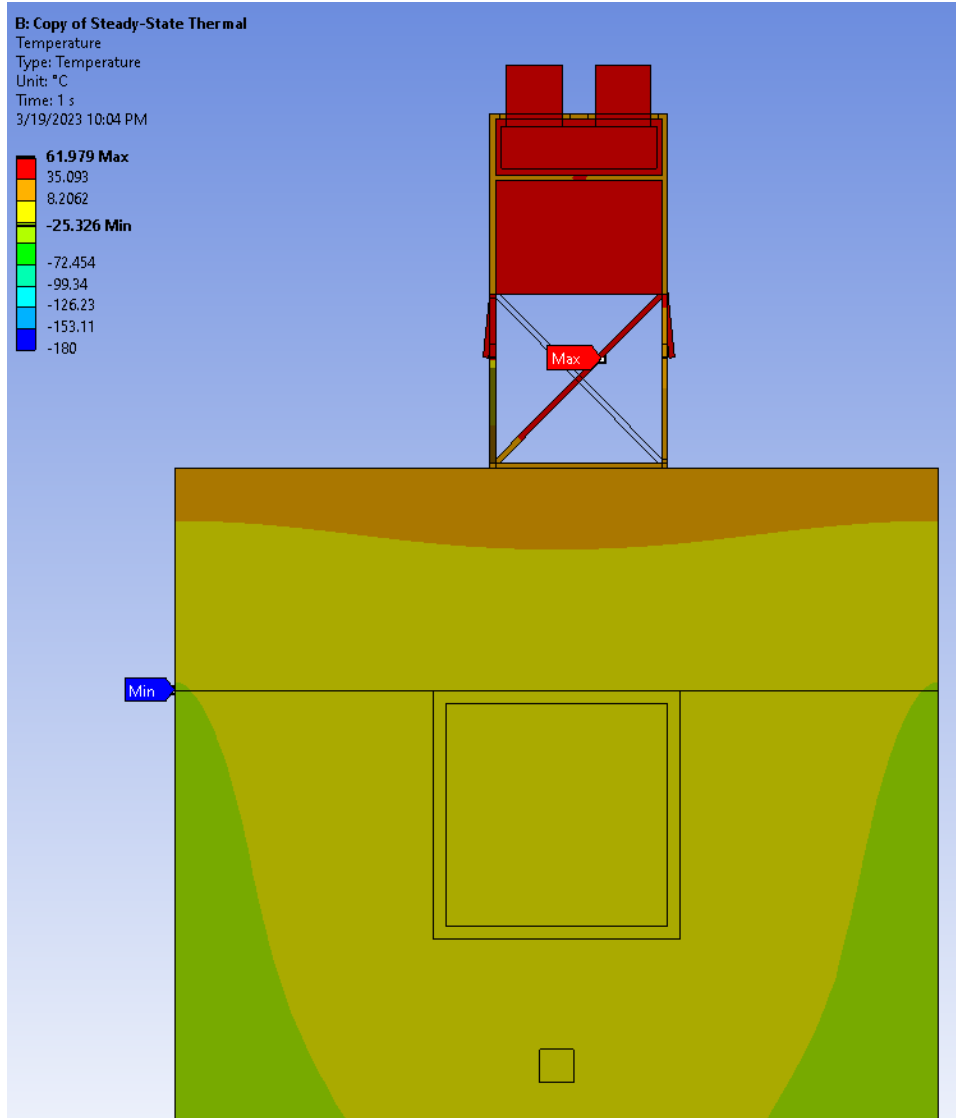
Figure 5.18 – Daytime battery, electronics, and optical module temperatures for TC2

5.4.3 TC3

Thermal control of a surface-based system is somewhat simpler than the other solutions. Heat is transferred from the battery and electronics module to the cover via thin polyethylene supports, thermal switches, and radiation. The large thermal mass of the battery provides thermal stability both at night and during daytime hours.
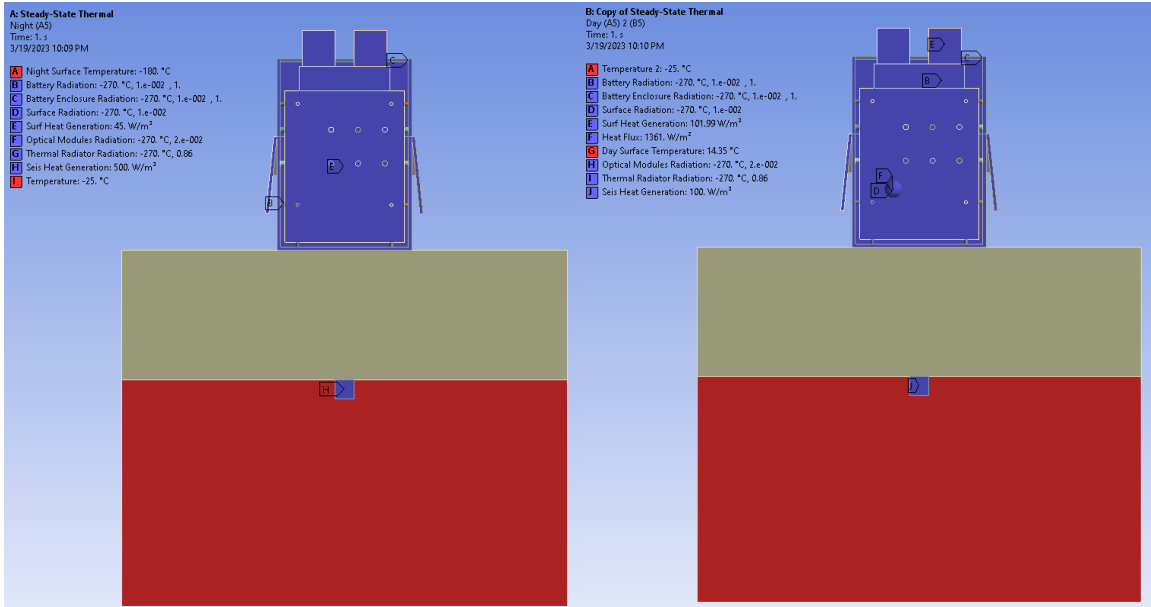
Figure 5.19– Night (left) and day (right) boundary conditions for TC3
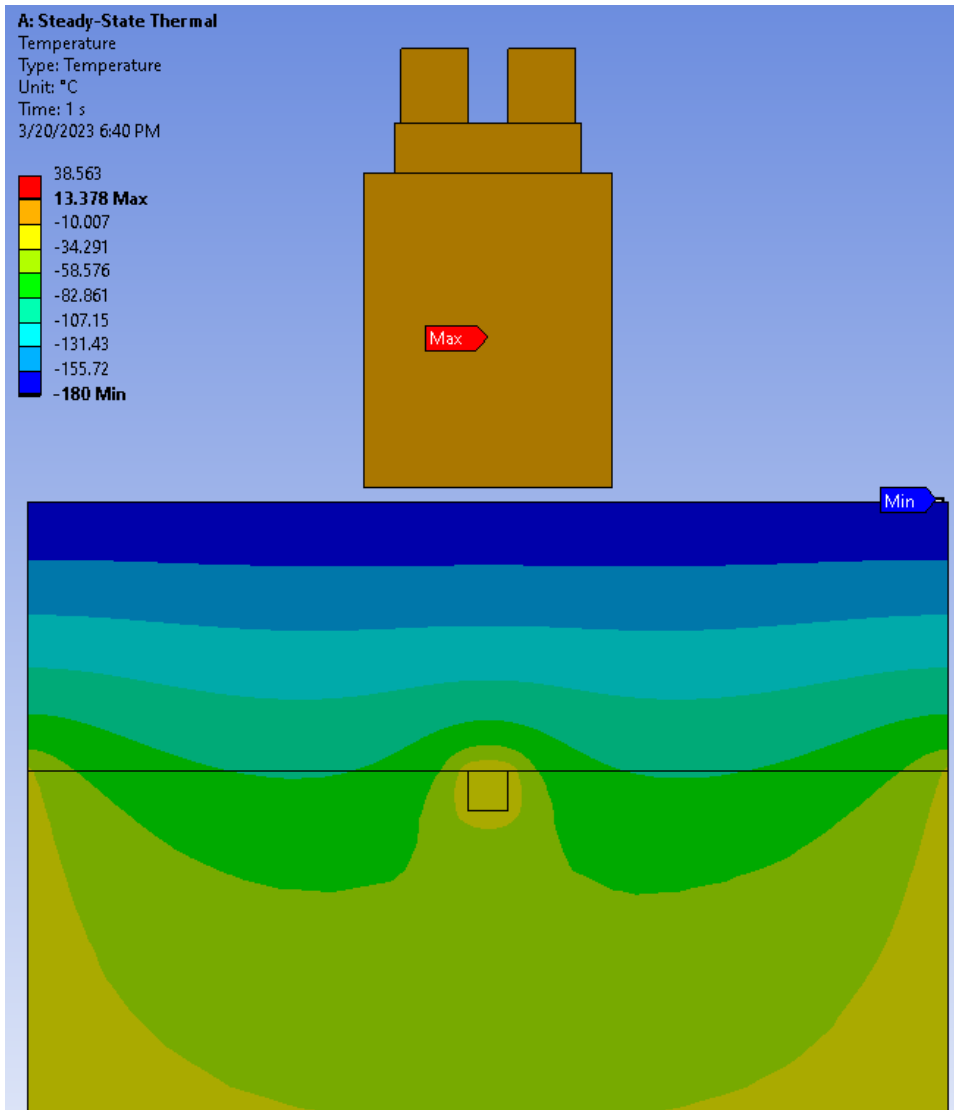
Figure 5.20 – Nighttime battery, electronics, and optical module temperatures for TC3
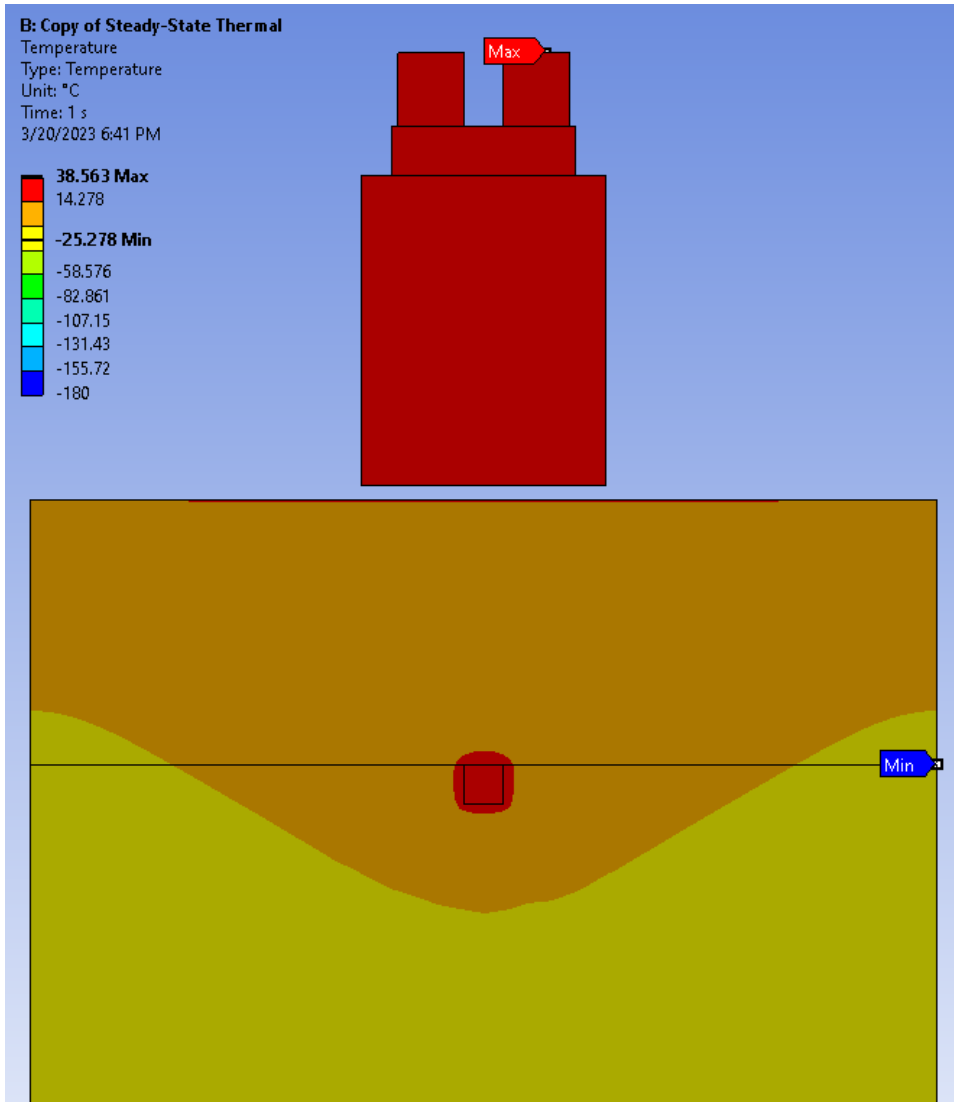
Figure 5.21 – Daytime battery, electronics, and optical module temperatures for TC3

5.5 Equator Analysis Results

Analysis for the equatorial designs closely follow the polar results. The reconfiguration of the location of the solar panels and optical modules had a minimal impact. The large increase in battery volume was the biggest factor.

5.5.1 TC4
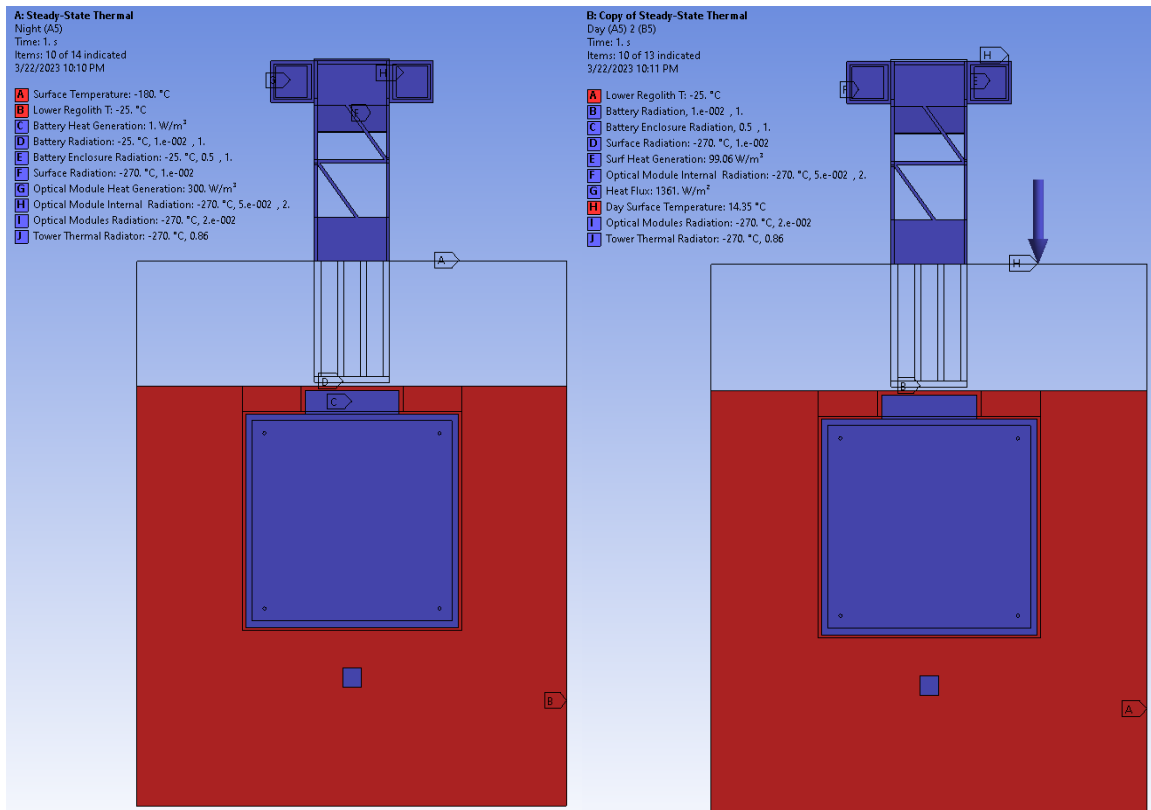
Figure 5.22– Night (left) and day (right) boundary conditions for TC4
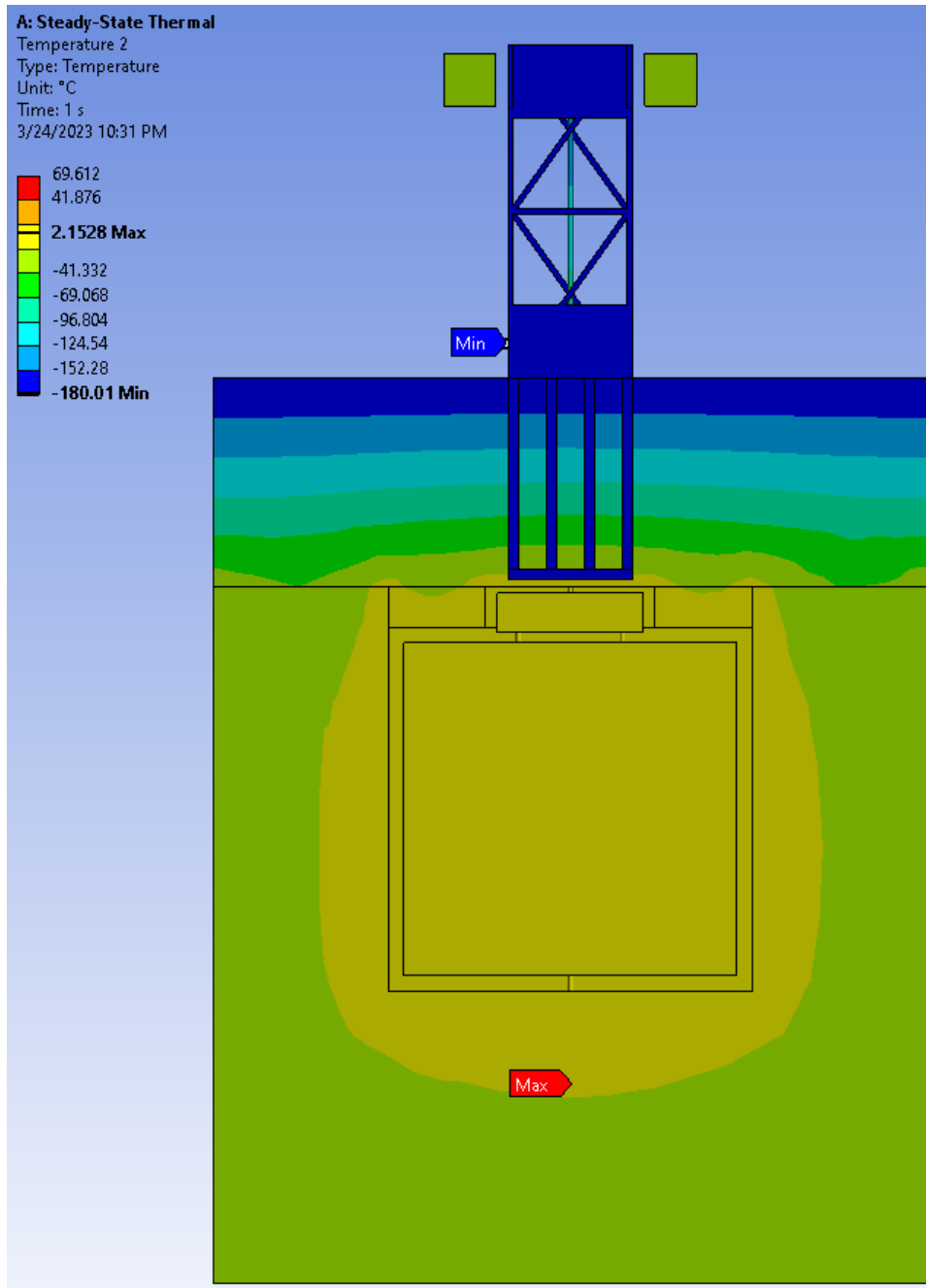
Figure 5.23– Nighttime battery, electronics, and optical module temperatures for TC4
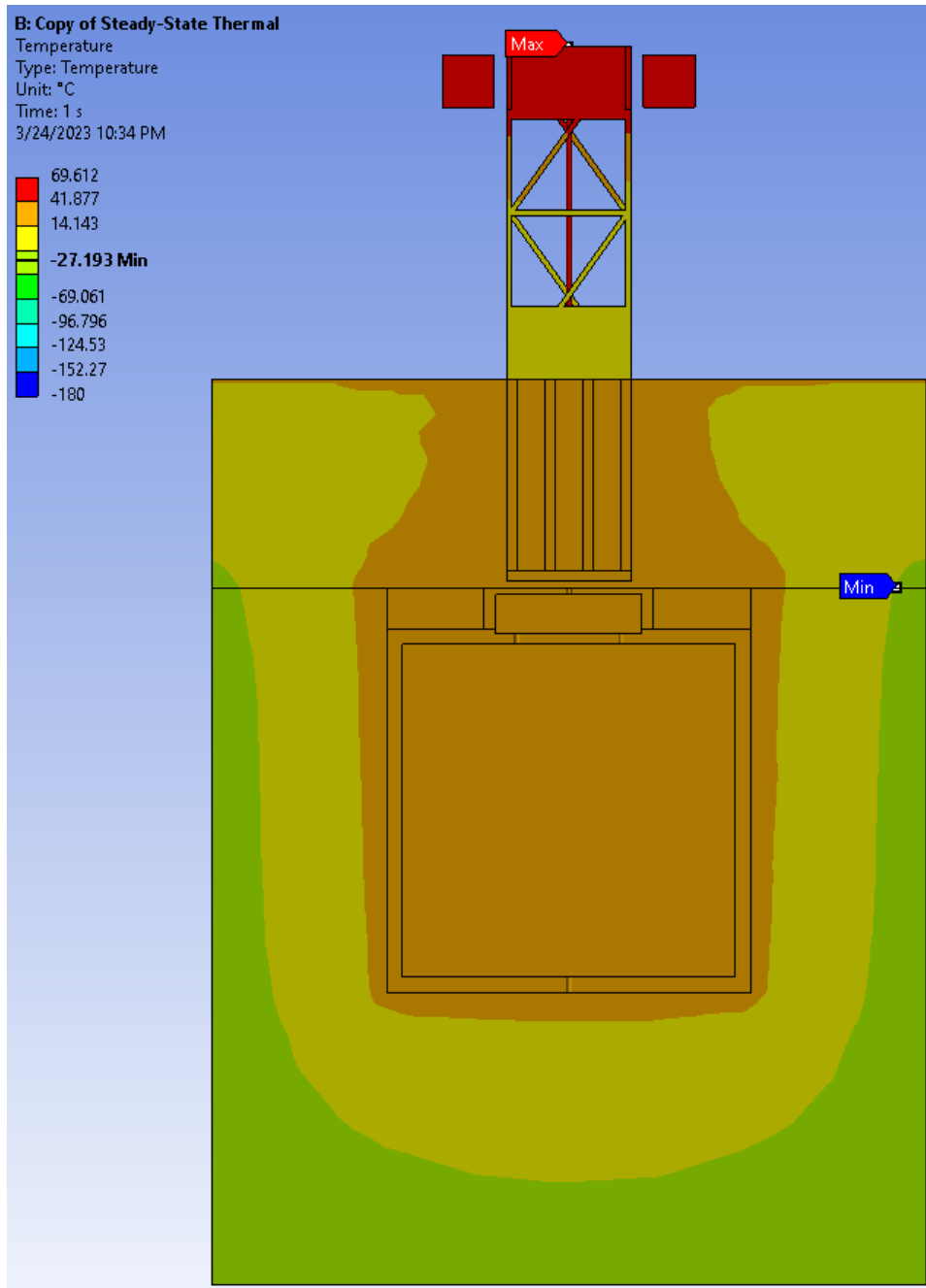
Figure 5.24 – Daytime battery, electronics, and optical module temperatures for TC4

5.5.2   TC5

A: Steady-State Thermal
Night (A5)
Time: 1. s
Items: 10 of 13 indicated
3/23/2023 9:23 PM

A Night Surface Temperature: -180. °C
B Sub Heat Generation: 3.74 W/m³
C Battery Radiation, 1.e-002 , 1.
D Battery Enclosure Radiation, 1.e-002 , 1.
E Surface Radiation: -270. °C, 1.e-002
F Surf Heat Generation: 550. W/m³
G Electrical Module Radiation: -270. °C, 5.e-002
H Optical Modules Internal Radiation, 1.e-002 , 2.
I Tower Thermal Radiator: -270. °C, 0.86
J Seismometer Heat Generation: 500. W/m³

B: Copy of Steady-State Thermal
Day (A5) 2 (B5)
Time: 1. s
Items: 10 of 14 indicated
3/23/2023 9:24 PM

A Heat Flux: 1361. W/m²
B Day Surface Temperature: 14.35 °C
C Sub Heat Generation: 0.1 W/m³
D Battery Radiation, 1.e-002 , 1.
E Battery Enclosure Radiation, 1.e-002 , 1.
F Surface Radiation: -270. °C, 1.e-002
G Surf Heat Generation: 1100.6 W/m³
H Electrical Module Radiation: -270. °C, 5.e-002
I Optical Modules Internal Radiation, 1.e-002 , 2.
J Tower Thermal Radiator: -270. °C, 0.86

Figure 5.25 – Night (left) and day (right) boundary conditions for TC5

A: Steady-State Thermal
Temperature
Type: Temperature
Unit: °C
Time: 1 s
3/23/2023 9:26 PM

61.979
35.089
8.1996
-18.69
-45.58
-72.469
-99.359
-126.25
-153.14
-180.03 Min
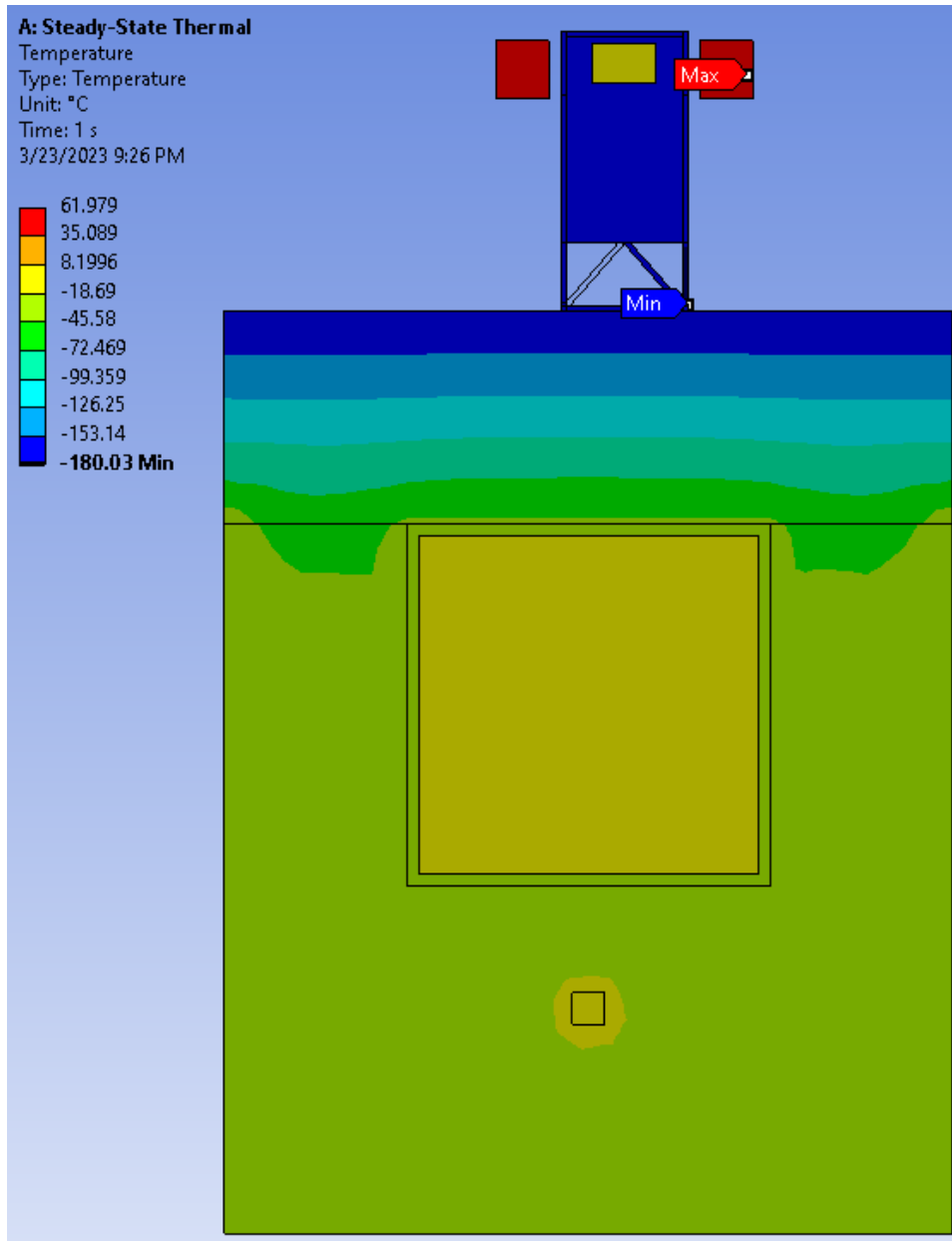
Figure 5.26 – Nighttime battery, electronics, and optical module temperatures for TC5
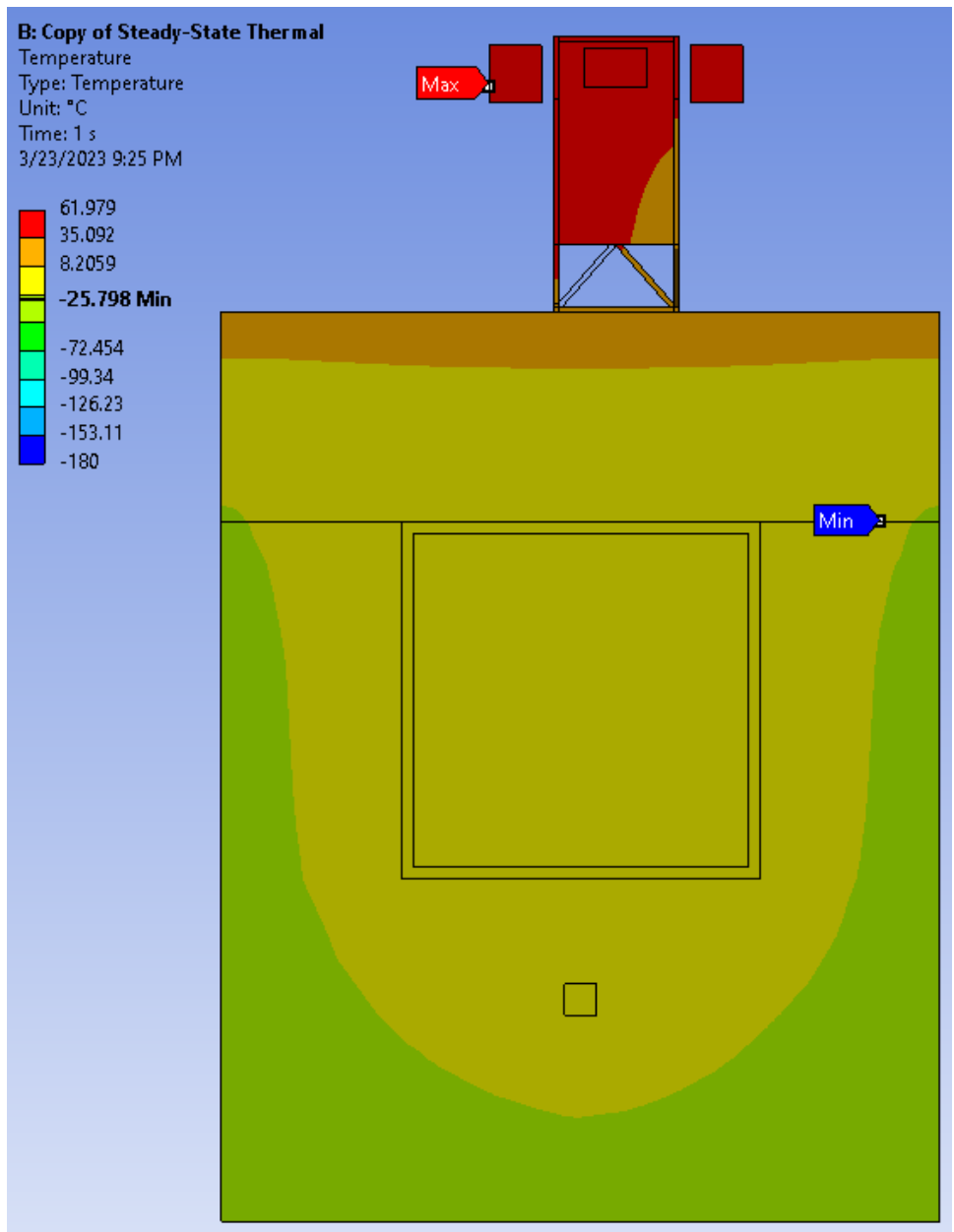
Figure 5.27 – Daytime battery, electronics, and optical module temperatures for TC5

5.5.3   TC6
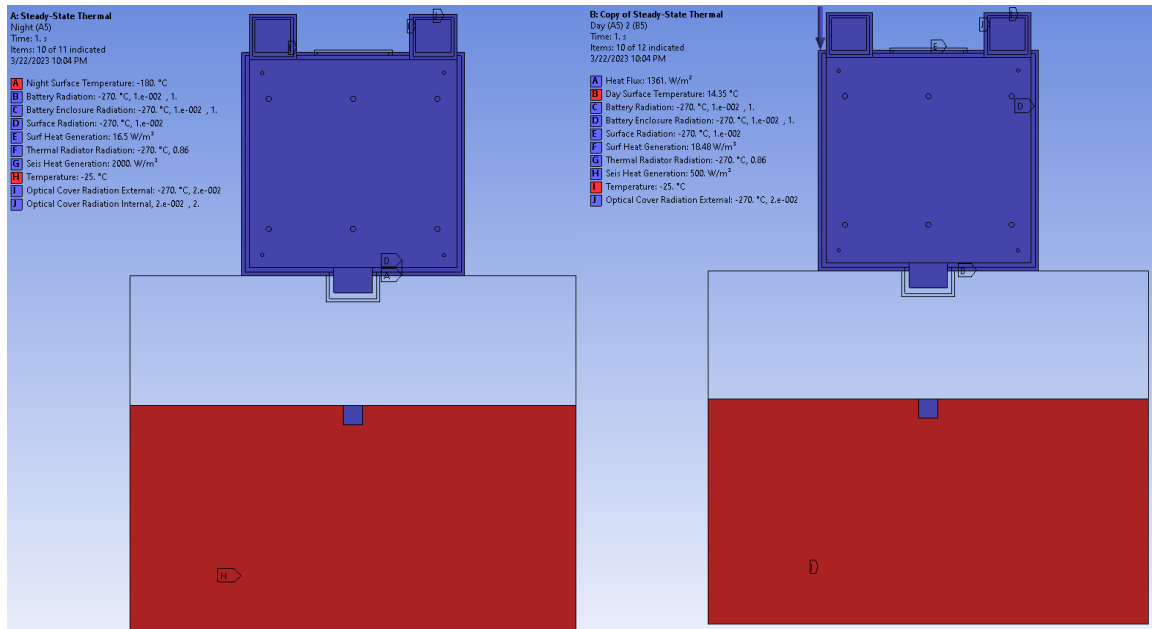
Figure 5.28 – Night (left) and day (right) boundary conditions for TC6
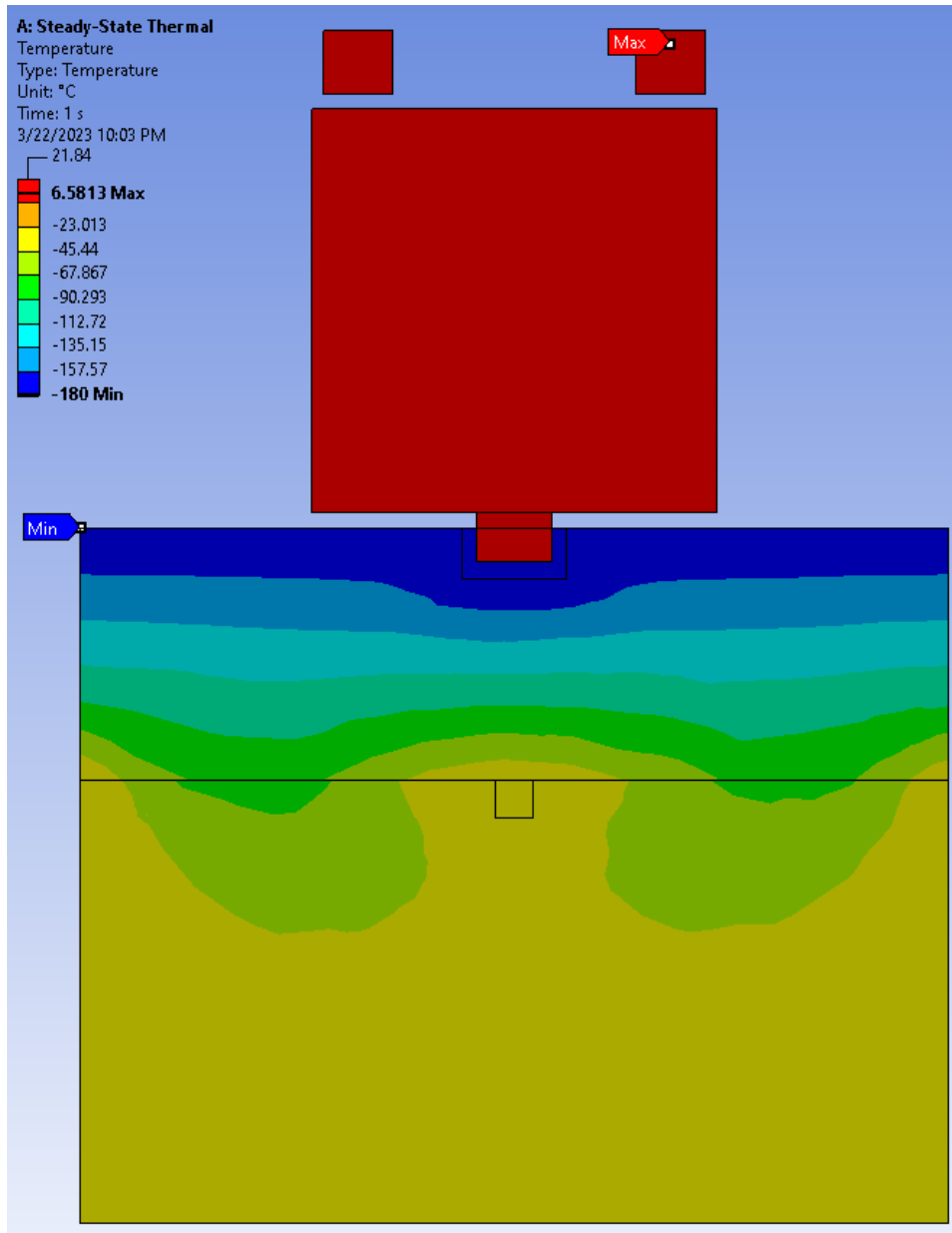
Figure 5.29 – Nighttime battery, electronics, and optical module temperatures for TC6
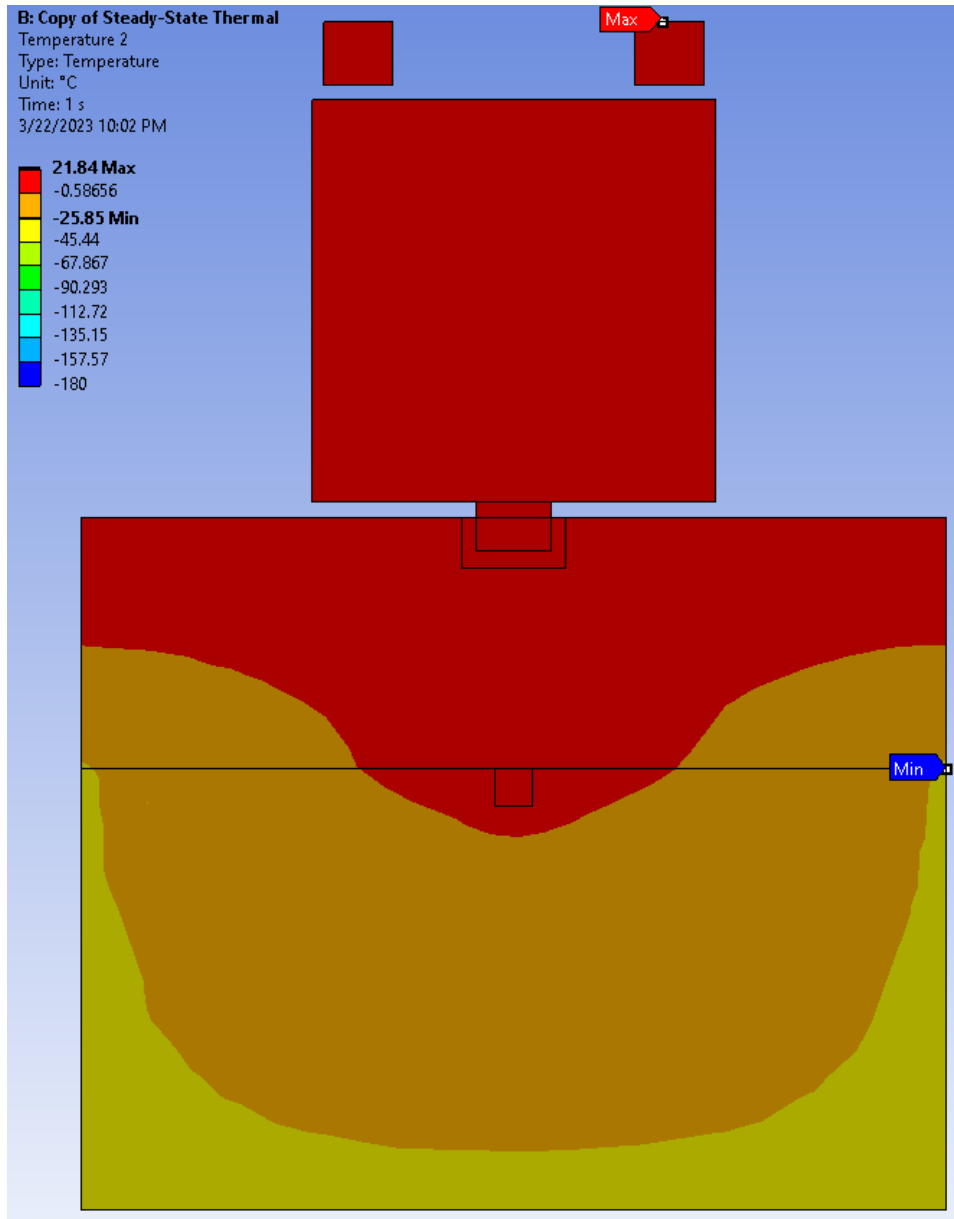
Figure 5.30 – Daytime battery, electronics, and optical module temperatures for TC6

5.6   Steady-State Temperature Results

During cold hours all thermal models were able to maintain minimum component operational temperatures using heating as needed, see Table 5.1 below. Models that included the electronics module above surface (TC2 and TC5) were not able to keep peek temperatures under maximums. As the thermal radiator for the test cases cannot easily be increased, special attention will be required for the integration of the optical communications modem which has a maximum operational temperature of 40°C. TC1 and TC3 exceeded the maximum subsurface temperature which was limited by the short period seismometer which has a maximum operational temperature of 20°C.

Table 5.1 – Operational and achieved temperatures

	Surface		Subsurface	
	Min [°C]	Max [°C]	Min [°C]	Max [°C]
TC1 Spec	-45	85	0	20
TC1 Result	-36.5	38.1	4.2	**31.7**
TC2 Spec	0	40	-25	20
TC2 Result	11.7	**59.2**	1.9	4.5
TC3 Spec	0	40	-30	20
TC3 Result	13.3	38.6	-12.7	**20.9**
TC4 Spec	-45	85	0	20
TC4 Result	-36.5	64.4	-1	20
TC5 Spec	0	40	-25	20
TC5 Result	4.4	**68.1**	-13.7	6.8
TC6 Spec	0	40	-30	20
TC6 Result	1.8	8.6	-28.8	7.5

6. Battery Utilization Analysis

6.1 Heater Power Consumption

Table 6.1 below shows a breakdown of the power consumption and generation. ANSYS Mechanical uses thermal generation per m^3, so the volumes of the surface and subsurface modules are included. Power consumption values are the values generated from the MATLAB power generation simulation (based on lines of visible communication) divided by the volume of the modules. Heat generation numbers are the iterated solutions that keep components within operational temperature ranges. By subtracting the consumption from the heat generation and multiplying by the module volumes, the total nighttime power consumption from heaters was calculated. During the day, any required heaters would run off solar power and so weren't included in the table.

Table 6.1 – Power consumption vs. heat generation

Temp Controlled Variables	TC1	TC2	TC3	TC4	TC5	TC6
Surface Heat Controlled Volume [m^3]	0.03	0.07	1.075	0.03	0.07	4.17
Subsurface Heat Controlled Volume [m^3]	0.04	1		0.04	4.096	
Seismometer Volume [m^3]	0.001	0.001	0.001	0.001	0.001	0.001
Day Surface Power Consumption [W/m^3]	436.3	1566.3	102.0	99.1	1100.6	18.5
Night Surface Power Consumption [W/m^3]	47.2	367.4	23.9	42.2	358.7	6.0
Day Subsurface Consumption [W/m^3]	2413.9	0.1		1851.8	0.0	
Night Subsurface Consumption [W/m^3]	607.6	0.1		596.0	0.0	
Seismometer Consumption [W/m^3]	100.0	100.0	100.0	100.0	100.0	100.0
Day Surface Total Heat Generation [W/m^3]	436.3	1566.3	102.0	99.1	1100.6	18.5
Night Surface Total Heat Generation [W/m^3]	300.0	367.4	45.0	300.0	550.0	16.5
Day Subsurface Total Heat Generation [W/m^3]	2413.9	0.1		1851.8	1.5	
Night Subsurface Total Heat Generation [W/m^3]	1000.0	15.0		1750.0	3.7	
Seismometer Heat Generation [W/m^3]	500.0	500.0	500.0	500.0	500.0	2000.0
Day Surface Heater [W]	0.0	0.0	0.0	0.0	0.0	0.0
Night Surface Heater [W]	7.6	0.0	22.7	7.7	13.4	43.7
Day Subsurface Heater [W]	0.0	0.0		0.0	6.2	
Night Subsurface Heater [W]	15.7	14.9		46.2	15.3	
Seismometer Heater [W]	0.4	0.4	0.4	0.4	0.4	1.9
Night Total [W]	23.7	15.3	23.1	54.3	29.1	45.6

Comparing the heater power consumption levels for the various configurations, the most power-hungry models are the models that include both the power electronics and the batteries subsurface, namely TC1 and TC4. This is because the larger subsurface thermal mass requires more heating to keep the sensitive electronics (optical communications modem) above minimums. Heating the battery along with the electronics leads to more conductive and radiative heating loss due to the large surface area of the battery cover. The configurations requiring the least amount of heating (TC2 and TC5) were the configurations with the battery subsurface and the electronics mounted to the tower. The configurations with all components (excluding seismometers) on the surface fell between the previous two groups, but landed near the power consumption levels for TC1 and TC4.

The MATLAB simulation was updated with the increased power load from the heaters and the simulation was used to calculate new battery capacities required to support the additional load. Tables 6.2 through 6.4 show the relative increase in kWh, mass, and volume. Pack capacities assume batteries operate between 20% and 100% state of charge. TC2 and TC5 required the smallest increase in size (54.5% and 116.5% respectively) while TC1 and TC4 required the biggest increase at 87.9% and 181.6% respectively.

Table 6.2 – Impact of heaters on battery capacity

	No Heater [kWh]	With Heater [kWh]
TC1	3.3	6.2
TC2	3.3	5.1
TC3	3.3	6.2
TC4	10.3	33.0
TC5	10.3	22.3
TC6	10.3	29.0

The pack mass and volumes were calculated using some general assumptions. It was assumed that the pack structure mass would work out to be 10% of the mass of the cells that make up the pack, the complete pack weighing 110% the weight of the cells alone. The pack volume was assumed to be 30% above that of the cells, the size of the battery being 130% of the cells alone. While these hard and fast rules may not be representative of real-world battery construction, they are applied evenly to all battery configurations allowing comparisons to be made.

Table 6.3 – Impact of heaters on pack weight.

	No Heater [kg]	With Heater [kg]
TC1	14.0	26.0
TC2	14.0	22.0
TC3	14.0	26.0
TC4	45.0	144.0
TC5	45.0	98.0
TC6	45.0	127.0

Table 6.4 – Impact of heaters on pack volume.

	No Heater [m³]	With Heater [m³]
TC1	0.8	1.5
TC2	0.8	1.2
TC3	0.8	1.5
TC4	2.5	8.0
TC5	2.5	5.4
TC6	2.5	7.0

When comparing the impact of the added power draw of heaters, battery systems designed to operate in equatorial latitudes are impacted more than twice as much as those at the poles. TC2 requires a 54.5% increase in volume compared to 87.9% for TC1 and TC3, a 33.4% difference. TC5 requires a 116.5% increase in volume compared to 220.4% and 181.6% for TC4 and TC6 respectively, a 103.9% and 65.1% difference. Batteries installed in equatorial latitudes stand to benefit the most in terms of mass and volume from using regolith to regulate battery cell temperature.

7. References

[1] Khatri, F.I., Robinson, B. S., Semprucci M.D., and Boronson, D.M., "Lunar Laser Communication Demonstration operations architecture," *Acta Astronautica,* Vol. 111, Jun 2015, pp. 77-83.

[2] Edwards, B., Randazzo, T., Babu, N., Murphy, K., Albright, S., Cummings, N., Ocasio-Perez, J., Potter, W., Roder, R., Zehner, S.A., Salah, R., Woodward, J., "Challenges, Lessons Learned, and Methodologies from the LCRD Optical Communication System AI&T," *2022 IEEE International Conference on Space Optical Systems and Applications (ICSOS)*, 2022, pp. 22-31.
https://doi.org/10.1109/ICSOS53063.2022.9749730

[3] Hemmati, H., Birnbaum, K. M., Farr, W. H., Turyshev, S., and Biswas, A., "Combined laser communications and laser ranging transponder for Moon and Mars," *Proceedings in Free-Space Laser Communication Technologies XXI,* SPIE, Vol. 7199, Feb 2009, pp. 167-178.

[4] Avdellidou, C., Munaibari, E., Larson, R., Vaubaillion, J., Delbo, M., Hayne, P., Wieczorek, M., Sheward, D., and Cook, A., "Impacts on the Moon: Analysis methods and size distribution of impactors," *Planetary and Space Science*, Vol. 200, No. 105201, 2021
https://doi.org/10.1016/j.pss.2021.105201

[5] Neal, C.R., Weber, R., and Seas, A., "The Lunar Geophysical Network, Final Report. Planetary Mission Concept Study," NASA, 2020.

[6] Vanoutryve, B., De Rosa, D., Fisackerly, R., Houdou, B., Carpenter, J., Philippe, C., Pradier, A., Jojaghaian, A., Espinasse, S., and Gardini, B.,. "An analysis of illumination and communication conditions near lunar south pole based on Kaguya Data," *Proceedings of 7th International Planetary Probe Workshop*, European Space Agency, Barcelona, Jun. 2010.

[7] Williams, J.-P., Paige, D.A., Greenhagen, B.T., and Sefton-Nash, E., "The global surface temperatures of the Moon as measured by the Diviner Lunar Radiometer Experiment," Icarus, Vol. 283, 2017, pp. 300–325.
https://doi.org/10.1016/j.icarus.2016.08.012

[8] Stopar, J., and Meyer, H., "Topographic Map of the Moon's South Pole (80° S to Pole)," Lunar and Planetary Institute, Regional Planetary Image Facility, 2019.

[9] Langseth, M. G., Keihm, S. J., and Peters, K., "Revised lunar heat-flow values," Lunar and planetary science conference proceedings, Vol. 7, Apr 1976, pp. 3143-3171.

[10] Lloyd, V., Johnson, A., Hambleton, K., "NASA Identifies Candidate Regions for Landing Next Americans on Moon," NASA, Release 22-089, Washington, DC, Aug 2022.

[11] Robinson B. S.,Boroson D. M., Burianek D. A., Murphy D. V., Khatri F. I., Burnside J. W., Kansky J. E., Biswas A., Sodnik Z., Cornwell D. M., "The NASA Lunar Laser Communication

Demonstration-successful high-rate laser communications to and from the Moon," Proceedings of SpaceOps, 2014, pp. 1685.

[12] Constantine S., Elgin L. E., Stevens M. L., Greco J. A., Aquino K., Alves D. D., and Robinson B. S., "Design of a high-speed space modem for the lunar laser communications demonstration," Proceedings in Free-Space Laser Communication Technologies XXIII, SPIE, Vol. 7923, Feb 2011, pp. 54-62.

[13] Cahoy, K., Grenfell, P., Crews, A., Long, M., Serra, P., Nguyen, A., Fitzgerald, R., Haughwout, C., Diez, R., Aguilar, A., Conklin, J., Payne, C., Kusters, J., Sackier, C., LaRocca, M., and Yenchesky, L., "The CubeSat laser infrared CrosslinK mission (CLICK)," Proceedings of the International Conference on Space Optics, ICSO. Vol. 11180, Jul. 2019, pp. 358-369.

[14] Yenchesky, L.K., Grenfell, P., LaRocca, M., and Cahoy, K., "Optomechanical design for CubeSat laser infrared crosslinks," *AIAA Scitech 2019 Forum*, 2019, pp. 0757.

[15] TESAT, "SCOT80 laser communications terminal for satellite networks," Jun. 2022.

[16] Bailey, S.H., Avenson, R., DellaGiustina, D.N., Zacny, K., Schmerr, N.C., Siegler, M.A., Bray, V.J., Murdoch, N., and Neal, C., "Lunar Seismometer and Burial System," (2019, April). Lunar Seismometer and Burial System. In 2019 SSA Annual Meeting (No. MSFC-E-DAA-TN67862).

[17] Yamada, R., Garcia, R. F., Lognonné, P., Kobayashi, N., Takeuchi, N., Nébut, T., and Ganepain-Beyneix, J., "On the possibility of lunar core phase detection using new seismometers for soft-landers in future lunar missions," Planetary and Space Science, Vol. 81, Jun 2013, pp. 18-31.

[18] Dubietis, A., and Arlt, R., "Periodic variability of visual sporadic meteor rates," Earth, Moon, and Planets, Vol. 106, No. 2, Jul 2010, pp. 105-111.

[19] Colombo, G., "Cassini's second and third laws," No. SAO SPECIAL REPT.-203, March 1966.

[20] Tooley, C. R., Houghton, M. B., Saylor, R. S., Peddie, C., Everett, D. F., Baker, C. L., and Safdie, K. N., "Lunar Reconnaissance Orbiter mission and spacecraft design," Space Science Reviews, 150(1), pp. 23-62, January 2010.

[21] Yost, B, and Weston, S, "State-of-the-Art Small Spacecraft Technology," 2021.

[22] Honeywell, "S-Band TT&C Transceiver," N61-1603-000-000, January 2016.

[23] AAC Clyde Space, "Power Conditioning & Distribution Units Starbuck-Mini," July 2020.

[24] Sparkwing, "Satellite Solar Panels," 150622, 2022.

[25] Dragonfly Aerospace, "Gecko Imager," retrieved 25 October 2022.
https://dragonflyaerospace.com/products/gecko/

[26] Eurotech, "COM-1289 PC/104 Tri-Band GPRS/GSM-R & 12-Ch GPS Receiver Board,"
ETH_COM-1289_DS071008, retrieved 25 October 2022.

[27] Bliley Technologies, "AR133 Series - Rubidium Frequency Standard," Rev 4, March 2020.

[28] AAC Clyde Space, "Command & Data Handling Sirius TCM LEON3FT," July 2020.

[29] AAC Clyde Space, "Power Conditioning & Distribution Units Starbuck-Micro," July 2020.

[30] Silicon Audio, "Low Noise Optical Seismic Sensor," retrieved 23 October 2022.

[31] Yamada R, Yamada I, Shiraishi H, Tanaka S, Takagi Y, Kobayashi N, Takeuchi N, Ishihara
Y, Murakami H, Yomogida K, Koyama J., Fujimura A., and Mizutani H., "Capability of the
penetrator seismometer system for lunar seismic event observation," *Planetary and Space
Science,* 57(7) pp. 751-763, June 2009.

[32] Nalbandian, R., "Micro-3 high precision low disturbance rotary actuator," *In Proc. 13th
European Space Mechanisms and Tribology Symposium–ESMATS,* 2009.

[32] Kreith, F., and Bohn, M. S., "Principles of Heat Transfer," 7th edition, St. Paul: West
Publishing Company, 1993.

[33] Lomax, H., Pulliam, T.H., Zingg, D.W., "Fundamentals of Computational Fluid Dynamics,"
Appl. Mech. Rev., 55(4), B61-B61, 2002.

[34] Samsung, "Specification of Product for Lithium-ion Rechargeable Cell Model Name:
INR18650-35E," Ver. 1.1, July 2009.

[35] Cheetham, B., "Cislunar autonomous positioning system technology operations and
navigation experiment (Capstone)," *ASCEND 2021,* 2021, p. 4128.

[36] Afshar-Mohajer, N., Wu, C. Y., Curtis, J. S., & Gaier, J. R., "Review of dust transport and
mitigation technologies in lunar and Martian atmospheres," Advances in Space Research, 56(6),
1222-1241, 2015.
https://doi.org/10.1016/j.asr.2015.06.007

[37] Gilmore, D. G., & Donabedian, M., "Spacecraft thermal control handbook," Aerospace
Press, Vol. 1, p. 163, 2002.